J-R BEHAVIOUR OF 20MnMoNi55 PRESSURE VESSEL STEEL

A THESIS SUBMITTED IN PARTIAL FULFILMENT OF THE REQUIRMENTS FOR THE DEGREE OF

Master of Technology

In

METALLURGICAL AND MATERIALS ENGINEERING

By

ARAVIND K

ROLL NO: 207MM112

DEPARTMENT OF METALLUGICAL AND MATERIALS ENGINEERING

NATIONAL INSTITUTE OF TECHNOLOGY, ROURKELA

2007-2009

J-R BEHAVIOUR OF 20MnMoNi55 PRESSURE VESSEL STEEL

A THESIS SUBMITTED IN PARTIAL FULFILMENT OF THE REQUIRMENTS FOR THE DEGREE OF

Master of Technology
In
METALLURGICAL AND MATERIALS ENGINEERING

By

ARAVIND K

ROLL NO: 207MM112

Under the Guidance of

PROF.B.B.VERMA

PROF.P.K.RAY

DEPARTMENT OF METALLURGICAL AND MATERIALS ENGINEERING

NATIONAL INSTITUTE OF TECHNOLOGY, ROURKELA

2007-2009

National Institute Of Technology
Rourkela

C E R T I F I C A T E

This is to certify that the thesis entitled, **"J-R BEHAVIOUR OF 20MnMoNi55 PRESSURE VESSEL STEEL"** submitted by Mr. **ARAVIND K** in partial fulfillment of the requirements for the award of Master of Technology Degree in **METALLURGICAL AND MATERIALS ENGINEERING** with specialization in **"METALLURGICAL AND MATERIALS ENGINEERING"** at the National Institute of Technology, Rourkela is an authentic work carried out by him under our supervision and guidance.

To the best of our knowledge, the matter embodied in the thesis has not been submitted to any other University / Institute for the award of any Degree or Diploma.

Dr. B.B.Verma
Professor & Head
Department of metallurgical and
Materials Engineering

Dr. P.K.Ray
professor,
Department of Mechanical
Engineering

Date:

Place:

ACKNOWLEDGEMENTS

This project is by far the most significant accomplishment in my life and it would be impossible without people who supported me and believed in me.

I would like to extend my gratitude and my sincere thanks to my honorable, esteemed supervisor **Dr. B.B.Verma,** professor & head, Department of Metallurgical and Material Engineering, and co-supervisor **Dr.P.K.Ray,** professor, Department of Mechanical Engineering, National Institute of Technology, Rourkela, for their invaluable guidance, constant encouragement and critical discussions throughout this research program and during the preparation of this thesis. Their inspiration at every stage of this work is duly appreciated..

I take this opportunity to acknowledge with sincere gratefulness to **Dr.Soumitra Tarafder**, Scientist F, Materials Science and Technology Division, National Metallurgical Laboratory, Jamshedpur for his initiative and inspiration and guidance to pursue this work.

I extend my gratitude and thanks to **Dr.N.Narasaiah**,Scientist , Fatigue and Fracture Group, Materials science and technology Division, National Metallurgical Laboratory, Jamshedpur, in carrying out round the cloak experiments, data analysis and his invaluable suggestions during technical discussions, sustained interest, moral support and encouragement without which it was impossible to carry out this investigation.

I am very much thankful to **Dr. S. Sivaprasad**, Scientist, National Metallurgical Laboratory and **Mr.Arpan Das**, Scientist, National Metallurgical Laboratory. Dr. S. Sivaprasad helped me a lot to understand and analysis the enormous testing data. I would like to thank Mr. Arpan Das, for giving me enthusiasm to work.

I would also like to thanks to Mr.Surajith Kumar Paul, and Mr.Tamshuk , PhD scholars, NML for their cooperation. I would also like to thank the entire Fatigue & Fracture Group, NML

Last but not least I would like to thank my parents, who taught me the value of hard work by their own example. They rendered me enormous support being apart during the whole tenure of my stay in NIT Rourkela.

ARAVIND K

CONTENTS

ABSTRACT

Material of Reactor Pressure Vessel (RPV) should have good fracture toughness to ensure safe operation of nuclear reactor. In order to be on safe side the fracture characteristics of RPV material have to be quantified. In this present work the fracture characteristics of 20MnMoNi55 steel – the material used for Indian PHWR – have been found using J-Integral test.

The microstructures of the steel and its relevant mechanical properties such as hardness and tensile properties have been characterized. Monotonic J-R curves of the material have been determined in the temperature of 23^0C and 300^0C. Fracture behaviour under quasi-static tearing load has been studied through fracture toughness tests on 20MnMoNi55 steel using Compact Tension(CT) specimens of Width(W)=50 mm and thickness(B)=20 mm. *J-R* curves were obtained from specimens precracked to $a/w = 0.5$ .The single specimen unloading compliance method have been used for generating J-R curves. Stretch zone widths (SZW) were measured on the fractured surfaces of broken specimens. The stretch zone dimensions that were determined have been used in conjunction with the experimentally derived *J-R* curve to obtain a value of the ductile fracture toughness parameter J_{SZW}. The initiation toughness, J_i, obtained at the intersection of the blunting line and the power-law fit to the *J-R* curve, and the critical toughness, J_Q, determined following the procedure of the ASTM standard, were estimated. The results of fracture studies under monotonic loading infer: (a) the material exhibits high fracture resistance at room temperature (b) the fracture resistance of the steel deteriorates at a temperature of 300^0C as compared to room temperature, the deterioration in the fracture properties has been attributed that steel exhibits embrittlement tendencies operative in this temperature. (c) The stretch zone formation is very prominent and starting/ending points are clearly discernible in 20MnMoNi55 steel. The correlation of J_{SZW}, critical toughness, (J_Q) and initiation toughness, (J_i), has been examined with a view to ascertain the applicability of the stretch zone dimension for measurement of fracture toughness.

LIST OF FIGURES

LIST OF TABLES

LIST OF SYMBOLS

Symbol	Description
a_N	Crack length up to machine notch
a	Crack length
a_0	Crack length after pre-cracking
B	Specimen thickness
B_N	Net Specimen thickness
B_{eff}	Effective specimen thickness
B	Remaining ligament after pre-cracking
C_1, C_2	Constant in J-Crack extension relation
$E, E^{/}$	Young's modulus, effective modulus
e_u	Percentage uniform elongation
e_t	Percentage total elongation
G	Crack extension rate
G_C	Elastic energy release rate
J	J-integral
J_{IC}, J_C	Critical J-integral strain energy release rate
J_i	Fracture initiation toughness
J_{el}, J_{pl}	Elastic and Plastic component of J
K, K_C	Stress intensity factor (SIF) , critical value of k
K_{IC}	Plane strain fracture toughness
m	Constant J-crack extension relation
P	Load
$p_{\max}$	Maximum load

V	Load line displacement
V_{pl}	Plastic component of clip gauge displacement
W	Specimen width
$\frac{\partial G}{\partial a}$	Rate of change of elastic energy release rate
Δa	Crack extension
ν	Poisson's ratio
σ	Stress
ε	Strain
Γ	Arbitrary contour around crack tip
σ_0	Flow stress
σ_{YS}	Yield strength
σ_{UTS}	Ultimate tensile strength
$\sigma_1, \sigma_2, \sigma_3$	Principal stresses
da/dN	Fatigue crack growth rate per cycle

LIST OF ABBREVIATIONS

Abbreviation	Description
ASM	American society of metals
ASME	American society of mechanical engineers
ASTM	American society for testing materials
CCL	Compliance crack length
COD	Crack opening displacement
CT	Compact tension specimen
CTOD	Crack tip opening displacement
DCPD	Direct current potential difference
DSA	Dynamic strain ageing
EPFM	Elastic plastic fracture mechanics
FCGR	Fatigue crack growth rate
FT	Fracture toughness
LBB	Leak before break
LT	Longitudinal-transverse direction
LEFM	Linear elastic fracture mechanics
LLD	Load line displacement
PHWR	Pressurized heavy water reactor
RA	Percentage reduction in area
RPV	Reactor pressure vessel
SEM	Scanning electron microscope
SL	Short transverse-Longitudinal direction
ST	Short transverse-Transverse direction
SZW	Stretch Zone Width
UTS	Ultimate tensile strength
YS	Yield strength

CHAPTER: 1

INTRODUCTION

The 20MnMoNi55 Steel of current interest is used in nuclear power plants. For the production of nuclear reactor pressure vessels. The operating temperature of this structural component is 28-300^{0}C .The pressure vessel and primary heat transport piping of nuclear power plants are designed and operated on the basis of leak before break (LBB) concept. In order to implement this LBB concept in the design of pressure vessels it is important to understand the fracture toughness behaviour of the material in its operating conditions.

It has 0.2 % carbon with 1.25% Mn, 0.5% Mo, 0.6% Ni with small quantity of Cr, Si and sulphur. From metallurgical point of view, increase of material strength may influence on the other properties such as toughness, corrosion resistance and may also affect the weldability. So good mechanical and metallurgical properties are required to withstand the internal pressure and prevent unexpected failure. The particular material 20MnMoNi55 steel has been the subject of extensive research work recently [1].

1.1 Nuclear Reactor

Most nuclear electricity is generated using reactors which were developed in the 1950s and improved since. New designs are coming forward and some are in operation as the first generation reactors come to the end their operating lives. Over 16% of the world's electricity is produced from nuclear energy.

A nuclear reactor produces and controls the release of energy from splitting the atoms of certain elements. In a nuclear power reactor, the energy released is used to make steam to generate electricity. In a research reactor the main purpose is to utilize the actual neutrons produced in the core. In most naval reactors, steam drives a turbine directly for propulsion. The principles for using nuclear power to produce electricity are the same for most types of reactor. The energy released from continuous fission of the atoms of the fuel is harnessed as heat in either a gas or water, and is used to produce steam. The steam is used to drive the turbines which produce electricity.

Pressure vessel or pressure tubes- Usually a robust steel vessel containing the reactor core and moderator/coolant, but it may be a series of tubes holding the fuel and conveying the coolant through the moderator.

1.2 Reactor Pressure Vessel

The RPV is cylindrical with a hemispherical bottom head and a flanged and gasketed upper head. The bottom head is welded to the cylindrical shell while the top head is bolted to the cylindrical shell via the flanges. The cylindrical shell course may or may not utilize longitudinal weld seams in addition to the girth (circumferential) weld seams. The body of the vessel is of low-alloy carbon steel. To minimize corrosion, the inside surfaces in contact with the coolant are clad with a minimum of some 3 to 10 mm of austenitic stainless steel. Numerous inlet and outlet nozzles, as well as control rod drive tubes and instrumentation and safety injection nozzles penetrate the cylindrical shell. The number of inlet and outlet nozzles is a function of the number of loops or steam generators [2].

1.3 Reactor Pressure Vessel material

In RPVs different materials are used for the different components (shells, nozzles, flanges, studs, etc.). Moreover, the choices in the materials of construction changed as the PWR products evolved. For example, the Westinghouse designers specified American Society for Testing and Materials (ASTM) SA 302 Grade the shell plates of earlier vessels and ASTM SA 53 Grade B Class 1 for later vessels. Other vessel materials in common use include American Society of Mechanical Engineers (ASME) SA 508 Class 2 plate in the USA, 22NiMoCr37 and 20MnMoNi55 in Germany, and 16MnD5 in France. SA-302, Grade B is a manganese-molybdenum plate steel used for a number of vessels made through the mid-1960s. Its German designation is 20MnMoNi55. As commercial nuclear power evolved, the sizes of the vessels increased. For the greater wall thicknesses required, a material with greater hardening properties was necessary. The addition of nickel to SA-302, Grade B in amounts between 0.4 and 0.7 weight per cent provided the necessary increased hardening properties to achieve the desired yield strength and high fracture toughness across the entire wall thickness. This steel was initially known as SA-302, Grade B Ni Modified.

Forging steels have also evolved since the mid-1950s. The SA-182 F1 Modified material is a manganese-molybdenum-nickel steel used mostly for flanges and nozzles in the 1950s and 1960s. Another forging material used then was a carbon-manganese-molybdenum steel, SA-336 Fl. Large forgings of these materials had to undergo a cumbersome, expensive heat treatment to reduce hydrogen blistering. Eventually these steels were replaced with steel, first described as ASTM A366 Code Case 1236 and are now known as SA-508 Class 2 that did

not require this heat treatment. This steel has been widely used in ring forgings, flanges and nozzles. It was introduced into Germany with the designation 22NiMoCr36 or 22NiMoCr37. With slight modifications, this steel became the most important material for German reactors for a long time. In addition, SA-508 Class 3 (20MnMoNi55 in Germany and 16 MnD5 and 18MnD5 in France) is used in the fabrication of RPVs.

Determination of initiation toughness in ductile materials is not straightforward, unlike in brittle materials, where the point of crack initiation is easily detectable due to sharp changes in the load carrying capacity of specimens being tested. The matter may be further complicated because of to variation of constraint attending crack tips. Fracture behaviour of ductile materials is usually characterized by elastic-plastic fracture parameters such as the *J*-integral, stretch zone width, crack tip opening displacement etc. The variations in these parameters with variation in constraint are often difficult to rationalize, particularly from the point of view that they are employed to represent material behaviour that are deemed to be universal, largely independent of test and specimen parameters. Often, the fracture resistance of materials obtained from testing standard specimens is not applicable to the fracture of components made of that material due to the difference in the constraint or triaxiality conditions at the tip of the crack in the two cases [3]. An attempt has been made to understand the nature of variation of fracture resistance parameters with change in crack length (i.e. with variation of constraint) in a pressure vessel piping material. The suitability of the parameters to represent the fracture toughness of materials, irrespective of the constraint condition, to which cracks in them are subjected. Details have been discussed in Chapter 2.

In ductile materials, fatigue precrack blunts on the application of load to accommodate plastic strains arising out of the local deformation processes at the crack tip. On continuation of loading, the blunting at the crack tip increases and reaches a limiting size, governed by the deformation capacity of the material, and further initiates a fracture (ductile crack) at its tip. On a ductile fracture surface, crack tip blunting is manifested as a featureless region known as the stretch zone. The stretch zone that forms during the process of ductile fracture can be thought of as a frozen imprint of the state of deformation at the instant of the critical event of ductile crack extension. Its extent can thus be used as a marker to indicate the corresponding fracture toughness parameter from the experimental resistance curve. Details have been discussed in chapter 2.

All the fatigue pre-cracking tests of the CT specimens that have been conducted are done at Room Temperature in constant ΔK mode using commercial software (Advanced Fatigue Crack Propagation, AFCP) on servo hydraulic testing machine of 50KN capacity. The crack lengths were measured by compliance technique using a COD gauge fitted on the load line of the specimen. All specimens were pre-cracked up to $a/W \approx 0.5$. The pre-cracked specimens were provided with a side groove of 20% of the specimen-thickness. The estimation of J-integral values of the fabricated specimens was carried out using an servo electric testing machine of 100KN capacity (INSTRON model: 8862). The single specimen unloading compliance technique has been used for evaluation of J-integral fracture toughness. These experiments have been carried out following the ASTM E 1820 standard. All tensile tests that have been conducted are done at room temperature and at $300^0 C$ by using a servo electric universal testing machine of 100KN capacity. The tensile tests have been done as per ASTM E8 standard. Details of test procedures, test conditions and factors affecting tests have been discussed in chapter 3.

The material studied is German steel, used in reactor pressure vessel of Indian PHWR and designated as 20MnMoNi55. Its yield stress is 490 MPa and the UTS are close to 620 MPa. The steel therefore is ductile in nature.

1.4 Objectives

The major objectives and the pertinent work-plan to fulfill these are categorized into three broad modules. These are:

(I) To characterize the microstructure and to determine the related mechanical properties of the selected steel.

Module I: This module consists of (a) determination of microstructure, (b) determination of hardness, (c) evaluation of tensile properties of the steel at Room temperature and at $300^0 C$

(II) To study the Monotonic fracture behaviour of the steel at ambient and at elevated temperatures.

Module II: This module comprises of (a) generation of monotonic J-R curves of the steel at Room temperature and at 300^{o}C temperature. (b) Evaluation of J_i and J_Q from J-R curve.

(III) To Study the formation of stretch zone width during ductile fracture and its correlation to the J-R curves.

Module III: This module comprises of (a), measurement of stretch zone width on the SEM images of side grooved 20MnMoNi55 fracture specimens which were tested at temperatures $28^0 C$ and $300^0 C$, (b)The Stretch Zone Width have been used in conjunction with the experimentally derived *J-R* curve to obtain a value of the ductile fracture toughness J_{SZW}.

CHAPTER: 2

LITERATURE REVIEW

2.1 Fracture mechanics

Fracture mechanics is the field of solid mechanics that deals with the behavior of cracked bodies subjected to stresses and strains. These can arise from primary applied loads or secondary self equilibrating stress fields (e.g. residual stresses).

Fracture (definition**) -** "It is defined as separation or fragmentation of body into two or more parts under the action of stress. The process of fracture can be considered to be made up of two components i.e. crack initiation and crack propagation. Fractures can occur under all service conditions. Material subjected to cyclic loading fail due to fatigue and material used at high temperature can fail due to creep rupture."

From investigating fallen structures, engineers found that most failure began with cracks. These cracks may be caused by material defects (dislocation, impurities...), discontinuities in assembly and/or design (sharp corners, grooves, nicks, voids...), harsh environments (thermal stress, corrosion...) and damages in service (impact, fatigue, unexpected loads...). Most microscopic cracks are arrested inside the material but it takes one run-away crack to destroy the whole structure.

To analyze the relationship among stresses, cracks, and fracture toughness, Fracture Mechanics was introduced. The first milestone was set by Griffith [4] in his famous 1920 paper that quantitatively relates the flaw size to the fracture stresses. However, Griffith's approach is too primitive for engineering applications and is only good for brittle materials.

For ductile materials, the milestone did not come about until Irwin [5] developed the concept of strain energy release rate *G* in 1950s.When the strain energy release rate reaches the critical value, the crack will grow. Later, the strain energy release rate was replaced by the stress intensity factor K with a similar approach by other researchers. After the fundamentals of fracture mechanics were established around 1960, scientists began to concentrate on the plasticity of the crack tips. In 1968, Rice [6] modeled the plastic deformation as nonlinear elastic behavior and extended the method of energy release rate to nonlinear materials. He showed that the energy release rate can be expressed as a path-independent line integral, called the J- integral. Rice's theory has since dominated the development of fracture mechanics in United States. Meanwhile, Wells [7], proposed a parameter called crack tip

opening displacement (CTOD), which led the fracture mechanics research in Europe. Thereafter, many experiments were conducted to verify the accuracy of the models of fracture mechanics. Significant efforts were devoted to converting theories of fracture mechanics to fracture design guidelines. Recent trends of fracture research include dynamic and time-dependent fracture on nonlinear materials, fracture mechanics of microstructures, and models related to local, global, and geometry- dependent fractures. Unlike existing major theories with a single-parameter approach (G, K, J, or CTOD), these recent research trends usually require more than one parameter to describe the behavior of the crack growth, which we will discuss later on.

2.2 Classification of Fracture Mechanics

Fracture mechanics can be classified in three types:

1. Linear Elastic Fracture Mechanics (LEFM) e.g. Glass.
2. Elastic Plastic Fracture Mechanics (EPFM) e.g. Mild steel.
3. Net Section Collapse (NSC) e.g. Aluminum.

In the regime where the global stress-strain response of the body is linear and elastic (LEFM), the stress intensity factor K is used. In the plastic collapse region, design can be done on the basis of ensuring that net section yield does not occur, whilst in the elastic-plastic region EPFM, nowadays called yielding fracture mechanics YFM, is applicable. The fracture characterizing parameters in YFM are the J-integral and the crack opening displacement, COD. All these fracture characterizing parameters meet both the Griffith energy criterion for fast crack growth, and the critical stress/strain criterion. For simple cases, fracture problems can be approached via the Griffith equation, which is particularly suitable for sharp cracks/defects in brittle materials

2.2.1 Linear Elastic Fracture Mechanics (LEFM)

Linear Elastic Fracture Mechanics (LEFM) first assumes that the material is isotropic and linear elastic. Based on the assumption, the stress field near the crack tip is calculated using the theory of elasticity. When the stresses near the crack tip exceed the material fracture toughness, the crack will grow. In Linear Elastic Fracture Mechanics, most formulas are

derived for either plane stresses or plane strains, associated with the three basic modes of loadings on a cracked body: opening, sliding, and tearing. Again, LEFM is valid only when the inelastic deformation is small compared to the size of the crack, what we called small-scale yielding. If large zones of plastic deformation develop before the crack grows, Elastic Plastic Fracture Mechanics (EPFM) must be used.

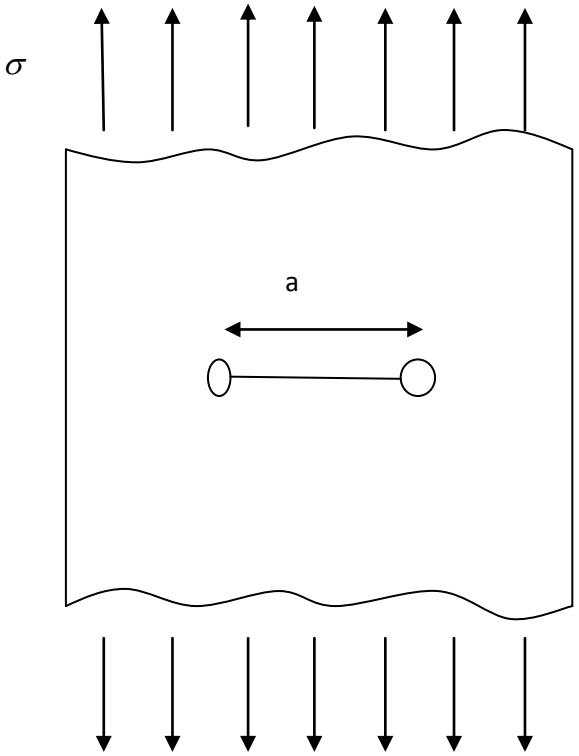

Figure 2.1: Linear elastic crack in tensile specimen

In case of Linear Elastic Fracture Mechanics (LEFM) we uses Stress Intensity Factor *K* or Stress Release Rate G.

Most metallic alloys and thermo set polymers are considered isotropic, where by definition the material properties are independent of direction. Such materials have only two independent variables (i.e. elastic constants) in their stiffness and compliance matrices. The two elastic constants are usually expressed as the Young's modulus E and the Poisson's ratio ν. However, the alternative elastic constants K (bulk modulus) and/or G (shear modulus) can also be used. For isotropic materials, G and K can be found from E and ν by a set of equations, and vice-versa.

2.2.1.1 Plane stresses and Plain strains

For the simplification of plane stress, where the stresses in the *z* direction are considered to be negligible, $\sigma_{zz} = \sigma_{yz} = \sigma_{xz} = 0$ the stress-strain compliance relationship for an isotropic material becomes,

$$\begin{bmatrix} \varepsilon_{xx} \\ \varepsilon_{yy} \\ \varepsilon_{zz} \\ \varepsilon_{yz} \\ \varepsilon_{zx} \\ \varepsilon_{xy} \end{bmatrix} = \frac{1}{E} \begin{bmatrix} 1 & -\nu & -\nu & 0 & 0 & 0 \\ -\nu & 1 & -\nu & 0 & 0 & 0 \\ -\nu & -\nu & 1 & 0 & 0 & 0 \\ 0 & 0 & 0 & 1+\nu & 0 & 0 \\ 0 & 0 & 0 & 0 & 1+\nu & 0 \\ 0 & 0 & 0 & 0 & 0 & 1+\nu \end{bmatrix} \begin{bmatrix} \sigma_{xx} \\ \sigma_{yy} \\ 0 \\ 0 \\ 0 \\ \sigma_{xy} \end{bmatrix}$$

For the case of plane strain, where the strains in the *z* direction are considered to be negligible $\varepsilon_{zz} = \varepsilon_{yz} = \varepsilon_{xz} = 0$ the stress-strain stiffness relationship for an isotropic material becomes,

$$\begin{bmatrix} \sigma_{xx} \\ \sigma_{yy} \\ \sigma_{zz} \\ \sigma_{yz} \\ \sigma_{zx} \\ \sigma_{xy} \end{bmatrix} = \frac{E}{(1+V)(1-V)} \begin{bmatrix} 1-V & \nu & \nu & 0 & 0 & 0 \\ \nu & 1-V & \nu & 0 & 0 & 0 \\ \nu & \nu & 1-V & 0 & 0 & 0 \\ 0 & 0 & 0 & 1-2\nu & 0 & 0 \\ 0 & 0 & 0 & 0 & 1-2\nu & 0 \\ 0 & 0 & 0 & 0 & 0 & 1-2\nu \end{bmatrix} \begin{bmatrix} \varepsilon_{xx} \\ \varepsilon_{yy} \\ 0 \\ 0 \\ 0 \\ \varepsilon_{xy} \end{bmatrix}$$

Three basic modes of loadings on a cracked body: opening, sliding, and tearing

There are three basic modes of crack tip deformation [8], the opening (Mode I), the in-plane shear (Mode II), and the out-of-plane shear (Mode III):

Mode I (Tension, Opening)

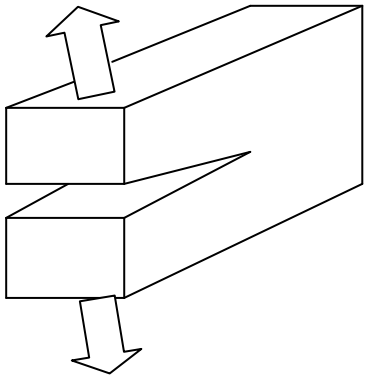

Figure 2.2: Opening mode deformation

Mode II (In-Plane Shear, Sliding)

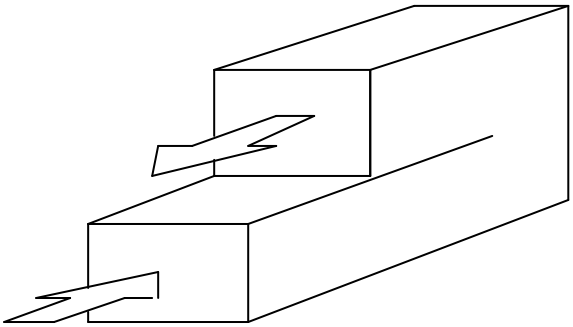

Figure 2.3: Sliding mode deformation

Mode III (Out-Of-Plane Shear, Tearing)

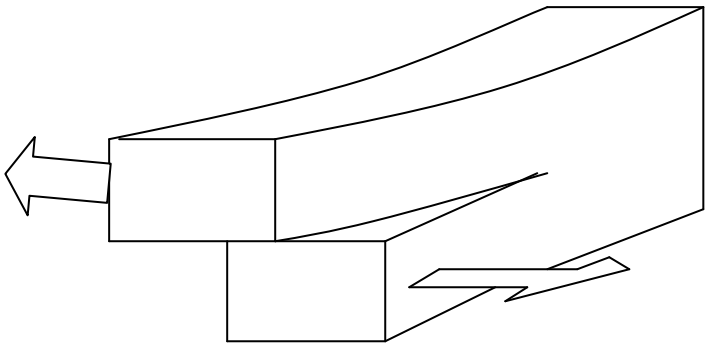

Figure 2.4: Tearing mode deformation

2.2.1.2 Stress Intensity Factor and Crack Tip Stresses

Crack tips produce a $\frac{1}{\sqrt{r}}$ singularity. The stress fields near a crack tip of an isotropic linear elastic material can be expressed as a product of $\frac{1}{\sqrt{r}}$ and a function of θ with a scaling factor K [8

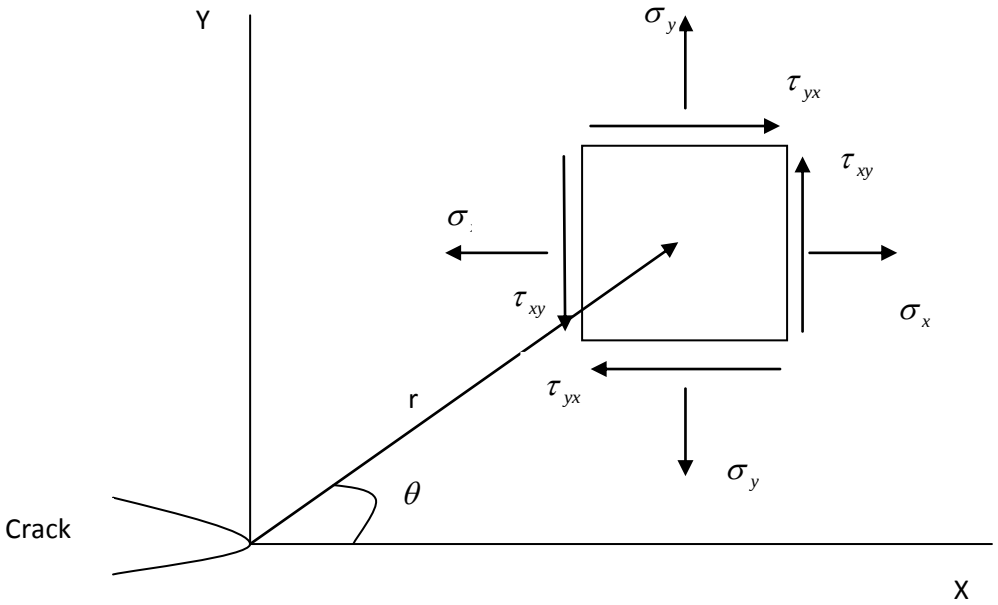

Figure 2.5: Stress field near crack tip of an isotropic linear elastic material

$$\lim \sigma_{ij_{y\to 0}}{}^{(I)} = \frac{K_I}{\sqrt{2\pi r}} f_{ij}{}^{(I)}(\theta)$$

$$\lim \sigma_{ij_{y\to 0}}{}^{(II)} = \frac{K_{II}}{\sqrt{2\pi r}} f_{ij}{}^{(II)}(\theta)$$

$$\lim \sigma_{ij_{y\to 0}}{}^{(III)} = \frac{K_{III}}{\sqrt{2\pi r}} f_{ij}{}^{(III)}(\theta)$$

Where the superscripts and subscripts *I*, *II*, and *III* denote the three different modes that different loadings may be applied to a crack. The factor K is called the Stress Intensity Factor.

2.2.1.3 Stress Intensity Factor and Fracture Toughness

Based on the linear theory the stresses at the crack tip are infinity but in reality there is always a plastic zone at the crack tip that limits the stresses to infinite values. It is very difficult to model and calculate the actual stresses in the plastic zone and compare them to the maximum allowable stresses of the material to determine whether a crack is going to grow or not.

An engineering approach is to perform a series of experiments and reach at a critical stress intensity factor K_C for each material, called the fracture toughness of the material. One can then determine the crack stability by comparing K and K_C directly.

2.2.1.4 Relationship between G and K

These two factors are directly related by the following formulas [9].

$$G = \frac{K^2}{E} \qquad \text{(Plane stress)}$$

$$G = \frac{K^2}{E}\left(1-\upsilon^2\right) \qquad \text{(Plane strain)}$$

The value of K for CT specimen

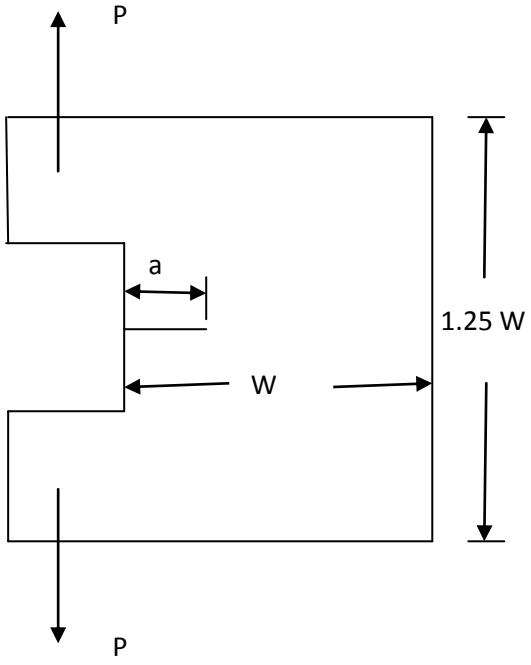

Figure 2.6: CT specimen with initial crack of length a

$$f\left(\frac{a_i}{W}\right)=\frac{\left[\left(2+\frac{a_i}{W}\right)\left(0.866+4.64\left(\frac{a_i}{W}\right)-13.32\left(\frac{a_i}{W}\right)^2+14.72\left(\frac{a_i}{W}\right)^3-5.6\left(\frac{a_i}{W}\right)^4\right)\right]}{\left(1-\frac{a_i}{W}\right)^{3/2}}$$

2.2.2 Elastic Plastic Fracture Mechanics (EPFM)

Linear Elastic Fracture Mechanics (LEFM) applies when the nonlinear deformation of the material is confined to a small region near the crack tip. For brittle materials, it accurately establishes the criteria for catastrophic failure. However, severe limitations arise when large regions of the material are subject to plastic deformation before a crack propagates. Elastic

Plastic Fracture Mechanics (EPFM) is proposed to analyze the relatively large plastic zones. Elastic Plastic Fracture Mechanics (EPFM) assumes isotropic and elastic-plastic materials. Based on the assumption, the strain energy fields or opening displacement near the crack tips are calculated. When the energy or opening exceeds the critical value, the crack will grow.

Although the term elastic-plastic is used in this approach, the material is merely nonlinear-elastic. In others words, the unloading curve of the so called elastic-plastic material in EPFM follows the original loading curve, instead of a parallel line to the linear loading part which is normally the case for true elastic-plastic materials.

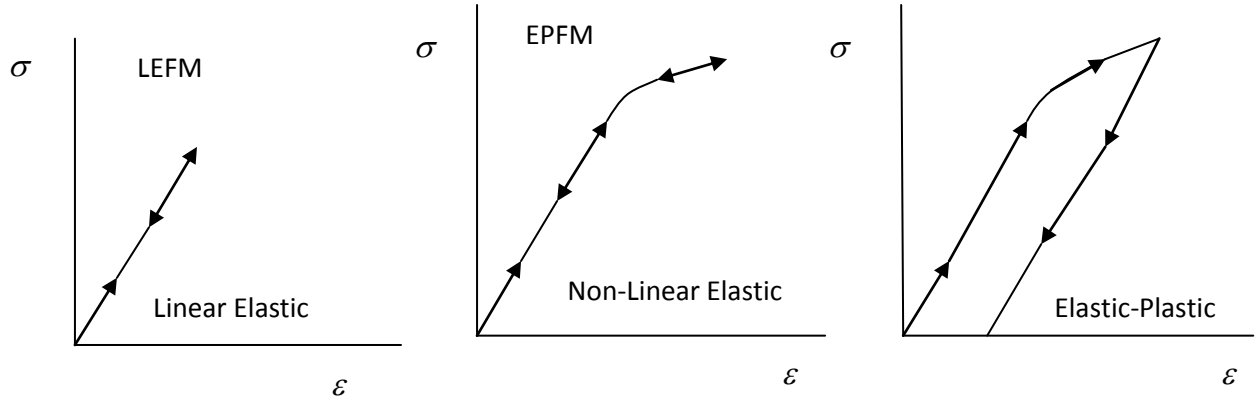

Figure 2.7: Difference between LEFM, EPFM

In case of Elastic Plastic Fracture Mechanics (EPFM) we use the J Integral or Crack Tip Opening Displacement (CTOD). Crack Tip Opening Displacement (CTOD) suggested by Wells, popular in Europe, and the J Integral proposed by Rice [6], widely used in the United States

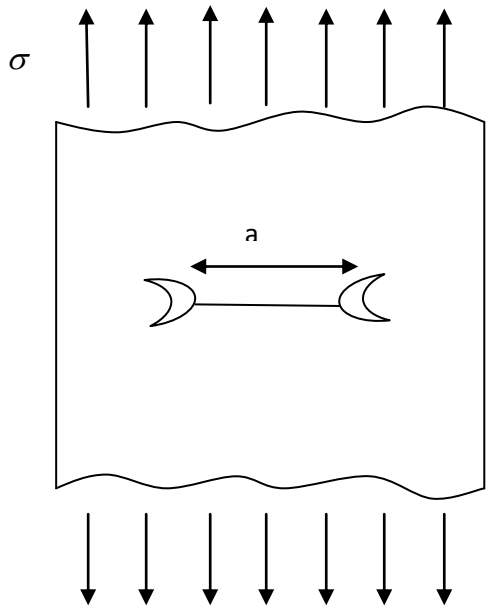

Figure 2.8: Elastic-plastic crack in tensile specimen

However, Shih provided evidence that a unique relationship between J and CTOD exists for a given material. Thus, these two parameters are both valid in characterizing crack tip toughness for elastic-plastic materials.

The basic EPFM analysis can be summarized as follows:

1. Calculate the J-integral or crack tip opening displacement (CTOD) δ as a function of the loading and the geometry.

2. The critical J-integral J_C or the critical CTOD δ can be determined empirically.

3. The J-integral J should NOT exceed J_C, or, the CTOD δ should not exceed the critical CTOD δ.

2.2.3 J-Integral

The *J*-Integral is employed as a fracture characterizing parameter for materials having elasto-plastic deformation idealized as non-linear elastic behaviour. Rice[6] applied deformation plasticity (i.e., non-linear elasticity) to the analysis of a crack in a non-linear material. He showed that the non-linear energy release rate, *J* could be written as a path independent line integral. Rice also showed that *J* uniquely characterizes crack tip stresses and strains in non-linear material. Thus the *J*-integral can be viewed as both energy parameter (strain energy release rate, *G*) and a stress intensity parameter (*K*) in the following fashion:

$$J = \frac{K_I^{\,2}}{E} = G \qquad \text{(Plane stress)}$$

$$J = \frac{K_I^{\,2}}{E}\left(1-\upsilon^2\right) = G\left(1-\upsilon^2\right) \qquad \text{(Plane strain)}$$

Definition of *J*-Integral

Rice [6] presented a path independent contour integral for the analysis of cracks. He then showed that the value of this integral, which he called *J*-Integral, is equal to the energy release rate in a non-linear elastic body that contains crack. Consider a non-linear elastic body containing a crack as shown in Fig. 2.9. Rice showed that the decrease in potential energy ΔU_P associated with the development of crack or void is given by,

$$-\Delta U_P = \int_{\Delta V} W dV - \int_{\Delta S} T \Delta u dS$$

For infinitesimal crack-extension, (co-ordinate system as per Fig. 2.8*)* the *J*-Integral is defined as:

$$J = \int_{\Gamma} w dy - T_i \frac{\partial u_i}{\partial x} ds$$

Where, $w = \int_{o}^{\varepsilon_{ij}} \sigma_{ij} d\varepsilon_{ij}$ is the strain energy density, $T_i = \sigma_{ij} n_j$ is the traction Vector, Γ is an arbitrary contour around the tip of the crack, *n* is the unit vector normal to Γ, σ, ε and *u* are the stress, strain, and displacement field, respectively[6].

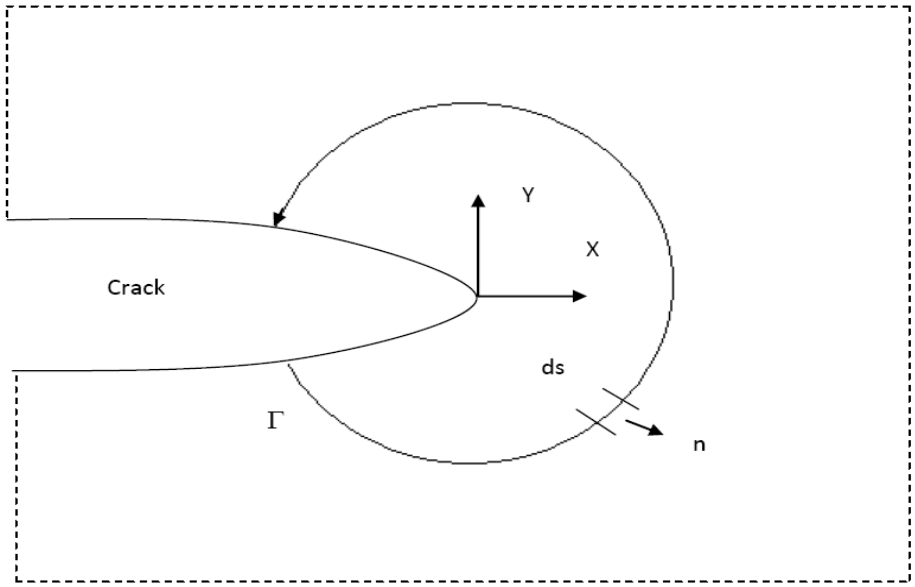

Figure 2.9 Crack in an arbitrary body—definition of *J*-integral

Rice, J. R showed that the *J*-integral is a path independent line integral and it represents the strain energy release rate of non-linear elastic materials:

$$J = -\frac{d\Pi}{dA},$$

Where, $\Pi = U - W$ is the potential energy, *U is* the strain energy stored in the body, *W* is the work done by external forces and *A* is the crack area.

In General, the *J*-integral for a variety of configuration can be written in the following form:

$$J = \frac{\eta U_C}{Wb}$$

Where η is dimensionless constant, W *is* specimen width, b=W-a, *a* is crack length and U_C is the area under load-displacement curve

The above equation can be separated into elastic and plastic components

$$J = \frac{\eta_{el} U_{C(el)}}{Wb} + \frac{\eta_P U_{C(P)}}{Wb}$$

The J-integral, represents a way to calculate work (energy) per unit fracture surface area in a material, Defines the point at which large-scale plastic yielding during propagation takes place under mode one loading. This value is difficult to determine experimentally, however in 1968 Jim Rice developed the J-integral test that allows one to calculate fracture toughness for materials in which sample sizes are too small (on the order of < 1 meter) for direct determination of Fracture toughness. Physically the J-integral is related to the area under curve of a load versus load point displacement

2.2.4 Crack Tip Opening Displacement (CTOD)

Definition of Crack Tip Opening Displacement-

There are two common definitions of the crack tip opening displacement (CTOD):

1. The opening displacement of the original crack tip.

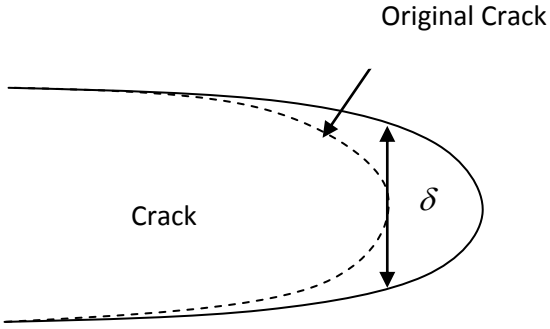

Figure 2.10a: CTOD of original crack tip

2. The displacement at the intersection of a 90° vertex with the crack flanks.

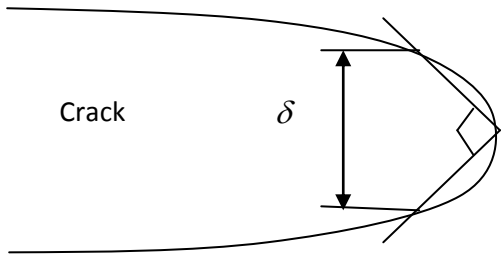

Figure 2.10b: CTOD of crack tip at intersection of 90 vertex

These two definitions are equivalent if the crack blunts in a semicircle

2.2.5 Relationship between *J* and CTOD

Consider a linear elastic body containing a crack, the J-integral and the crack tip opening displacement (CTOD) has the following relationship

$$J = \frac{K^2}{E} = m\sigma_{ys}\delta$$

Where σ_{ys} is the small scale yielding stress and m is a dimensionless constant that depends on the material properties and the stress states. For plane stress and non hardening materials, m = 1. Hence, for a through crack in an infinite plate subjected to a remote tensile stress σ (Mode I), the crack tip opening displacement δ is

. $$\delta = \frac{G}{\sigma_y} = \frac{J}{\sigma_y}$$

2.2.6 J-R Curve

The J- resistance curves are used for characterizing the elastic-plastic fracture behavior of metallic components. They are usually determined from ASTM E-1820 standard specimens. The stress multi triaxiality, 'q', ahead of the crack tip plays an important role in determining fracture resistance behavior of components. ligament. The J-R curve depends on component level. The J-R curve is mainly influenced by the multiaxiality of stress state across the

For thin sheets resistance to crack growth R increases as the crack grows from its initial length as shown in the Fig.2.2. In this case instability occurs when a line of G_1 at constant load becomes tangent to the R-curve, i.e.

$$G_1 = R$$

and

$$\frac{\partial G_1}{\partial a} = \frac{\partial R}{\partial a}$$

The idea of a crack growth resistance or R-curve was first suggested by Krafft et al. [9]. These investigators postulated that the crack resistance curve should have a unique shape for each material independent of initial crack length, specimen geometry and boundary loading conditions. This concept is expressed in terms of stress intensity factor, K_C and K_R as given in Fig.2.11. The critical stress intensity factor, K, is that at which tangency between K_R and K_C occurs. In making the estimate of K_C, R curves are regarded as though they are independent of the initial crack length a_i and the specimen [10].

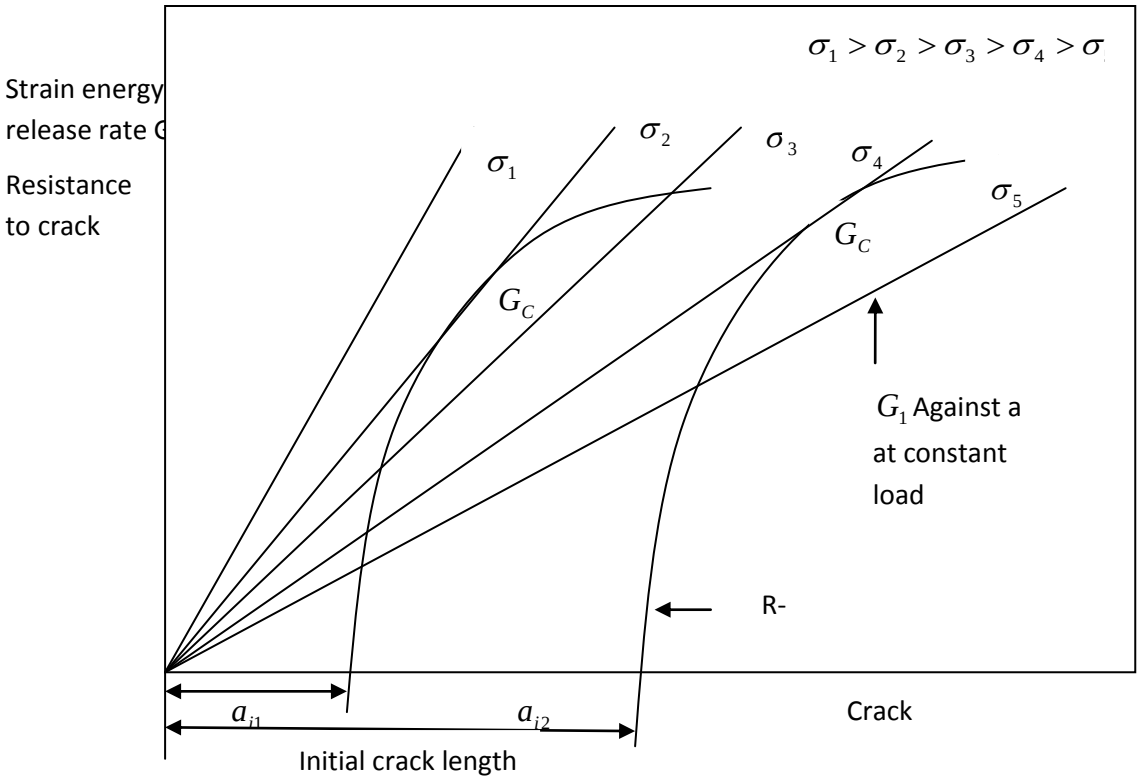

Figure 2.11(a): R-curves in terms of G for a specimen containing initial crack a_{i1} and a_{i2}

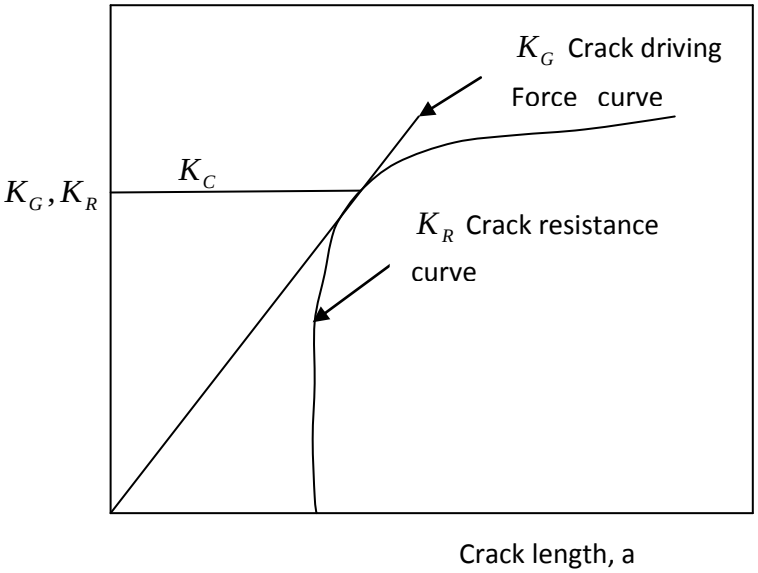

Figure 2.11(b): R-curve in terms of stress intensity factor

2.3 Limitations of Single Parameter Characterization

Under small scale yielding conditions a single parameter (i.e. J-integral) characterizes the crack tip conditions and can be used as geometry independent fracture criterion. However, the single parameter assumption is rigorously correct only in an infinite body. In a finite body, the single parameter assumption is suspect when the plastic zone size is significant compared to the dimensions of the body or crack. The breakdown of single parameter fracture mechanics is gradual from low to higher load levels in highly constraint geometries such as deeply cracked bend specimens. But it occurs at relatively low load levels in low constraint geometries such as cracked specimens in uniaxial tension. Now, there is general agreement that single parameters approach is limited to high constraint geometries.

In most cases, standard ASTM specimens maintained high constraint even up to high load levels. ASTM standards require both sufficient thickness to ensure predominantly plane strain conditions at the crack tip and a crack depth of at least half the specimen width. Within certain limits on load level and crack growth, these restrictions ensure the existence of high constraint conditions for fracture and the single parameter characterization is valid. However, actual structures are generally low constraint geometries. This difference between crack tip constraint between specimens and structures indicates that structures can often carry greater loads without failure predictions using fracture toughing values which are measured from

laboratory specimens. This introduces a high degree of conversation into the design of load carrying of components. Experiment techniques have been developed for measuring the apparent fracture toughness of low constraint geometries. This work has shown that slope of the J-R curve. The slope of the J-R curve will effect on the load and associated crack growth of components. As crack tip constraint plays important role in explaining geometric dependence of J-R curve, it seems worthwhile to discuss the underlying idea and physical significance of constraint

2.4 Physical Significance of Crack Tip Constraint

Constraint is a structural feature that inhibits plastic flow and causes a higher triaxiality of stresses. Therefore, it promotes because the input of external work, for example, measured by J will to a lesser part be dissipated by plastic deformation but be available to enhance material degradation and damage. High crack tip constraint is often found in specimens with sufficiently deep crack under predominantly bending load. Low constraint is often associated with specimen of relatively shallow cracks under predominantly tensile loading. Low constraint generally manifests itself in high crack tip ductility and high fracture toughness.

Although there is no doubt that the resistance against ductile tearing depends on crack tip constraint, the problem still to be solved in how to define and quantify this parameter significant, reliable and reproducible manner. Different definitions and measures are in use and two parameter fracture mechanics has emerged in which second parameter is used to quantify crack tip constraint.

2.5 Two Parameter Fracture Mechanics

The development and confirmation of proper fracture criteria fro crack initiation and stable crack growth has been one of the most important objectives in the study of elastic plastic fracture mechanics. The J-integral has played an important role in fracture mechanics and engineering application over the past 20 years as a single parameter to characterize the crack tip stress field. It was considered the most appealing parameter for crack initiation and stable crack growth. Deformation plasticity solutions which elucidate the behavior of a stationary crack under plane stress or plane strain solutions were given by the Hutchinson and Rice and Rosengren model, known as HRR singularity fields. The amplitude of these is given by J-integral. The conditions under which the HRR fields correspond to those found in small scale

yielding (SSY) as characterized by the J-integral are referred to as the conditions of J-dominance characterized of the crack tip field.

Crack initiation and stable crack growth in ductile material are usually described by J-R curves obtained from standard fracture specimens. The original idea was that J-integral can be used to characterize the crack tip stress field and one unique fracture resistance is sufficient to characterize the material. However, there is growing evidence showing that the J-R curve depends on specimen size, geometry and loading mode. Therefore, the transferability of specimen J-R curve to component level is an unresolved issue that receives a lot of attention among researchers. The J-R curve is mainly influenced by the multiaxiality of stress state across the ligament. The multiaxiality can be determined by finite element calculations for specimen and components. By comparing the multiaxiality values of specimen and components, it is possible to assess component fracture behavior correctly.

2.6 Effect of Chemical Composition on fracture toughness

Preamble

The chemical composition and their percentage in the steel mostly influence the fracture property of steel. The alloying elements are substitutional and interstitial solutes, the both have detrimental effect on the impact properties of steel except nickel, especially the interstitial solutes. The solutes have other effect such as altering the ferrite-pearlite ratio, refining the ferrite grain size by decreasing the transformation temperature on cooling (i.e. manganese), producing precipitation effect (i.e. carbon and nitrogen) and withdrawing interstitials from solution (i.e. aluminum). The controlling the critical amount of these alloying elements is very necessary for obtaining desired fracture property in steel. The most commonly alloying elements used in high strength steel are C, Si, Mn, Mo, V, Al, Ni, Cu, S and P their effect are discussed below.

2.6.1 Carbon

The carbon is the most important alloying element which influences the fracture property of the steel. Carbon increase cause formation of cementite phase which increases the hardness and strength of steel but the cost of toughness properties, so for design of structural steel for maximum toughness, carbon should maintain to the minimum level needed to achieve the desired strength. In early nineties the steel is mainly designed on the based upon

the tensile strength and little consideration of yield stress, weldability or toughness. The joining method for structural steel was riveting and the carbon contents of the order of 0.3%. When the welding comes as measure joining method for steel then, the weldability of steel was improved by lowering the carbon content below 0.2%, without affecting the strength by adding other alloying element like Mn, V and Al etc. The low carbon steel has ferritic with low amount of pearlite, so it has good ductility and toughness.

2.6.2 Silicon

Silicon is one of the common deoxidizers used during the process of manufacture. The effect of Si on the transition temperature of low carbon steel is described by Equation [11,12] 1% increase in Si increases the transition temperature by 44°C, Thus , it is necessary to kept Si as minimum as possible to get good toughness properties.

$$\mathrm{ITT^{o}C} = -19 + 44(\mathrm{Si}) + 700\left(\sqrt{\mathrm{N_f}}\right) + 2.2(\mathrm{pearlite}) - 11.5d^{-1/2}$$

2.6.3 Manganese

The all the steel manganese use as deoxidizer, and improved the strength of low carbon steel. The effect of Mn addition comes as comparable grain refinement which results in decrease in transition temperature. Each 0.1% increase in Mn decrease the transition temperature by 5^0C. The Mn is used in low carbon steel up to 1.65%, above this the steel tends to become air hardened, with resultant impairing of the ductility. Manganese levels above those required for hardenability and sulphide formation may be detrimental, particularly in martensitic steel with carbon content excess of 0.30 to 0.35 %. The study on 0.032% C steel with Ni between 7 to 9 % and Mn between 0.6 to 6 % [13]. Ni reductions with Mn levels at 2 % lead to an increase in toughness. However the best Charpy toughness 101 J at -60^0C, was recorded with Mn at 0.6 % and Ni at 6.6 % as predicted by the model. It was found that once Ni exceeds a critical point, which depends on Mn concentration, toughness decreases.

2.6.4 Molybdenum

Molybdenum is carbide former, it form complex carbides $(FeMo)_{6C}$, $Fe_{21}Mo_2C_6$. The decrease in carbon content or by substituting it into fine M_2C carbides through increasing molybdenum content is improved the yield strength, tensile strength and lowered DBTT of the steels [14]. The presence of Mo alone in the range of 0.817-0.881 wt % resulted in decreased FATT and an increase of impact toughness [15]. The beneficial effect of Mo is due to formation of predominant AF (about 70-75%) and Granular Banite (GB) (20 %), at the

expense of ferrite with second phase FS (A) and grain boundary ferrite (GBF) in weld metal. Molybdenum tends to help steel resist softening at high temperatures and is an important means of assuring high creep strength.

2.6.5 Nickel

Generally, with respect to both toughness and transition temperature, nickel is beneficial to steel with less than about 0.40% C. At carbon contents above 0.40%, nickel additions in excess of about 1.5 % are not effective. Steels utilize the effect of nickel content in reducing the impact transition temperature, thereby improving toughness at low temperatures. For applications involving exposure to temperatures from 0 to $-190^0 C$, the ferritic steels with high nickel contents are typically used. Such applications include storage tanks for liquefied hydrocarbon gases and structures and machinery designed for use in cold regions. The 5% Ni steel retains relatively high fracture toughness at $-162^0 C$ and the 9% Ni steel retains relatively high fracture toughness at $-196^0 C$ [15]. These temperatures approximate the minimum temperatures at which these steels may be used.

2.6.6 Nitrogen

Nitrogen is present in steel in free form; it is good grain refiner and improves the yield strength of the steel by precipitation effects, but it solubility is limited. Also N drastically increases the transition temperature it is observed from the equation (3.3).

2.6.7 Sulphur and Phosphorus

Small amount less than 0.005% Sulphur and Phosphorus is always present in the steel. It improves the machinability and atmospheric corrosion resistance property respectively. But it is very detrimental effect on the toughness and transition temperature of steel. Sulphide inclusions decrease K_{IC} by prompting crack or void nucleation. The 20 J Charpy V-notch transition temperatures is raised about $7^0 C$ for each 0.01% phosphorus. The combined effect of this alloying elements described by the carbon equivalent (CE) of the steel. It describes the behaviour of phase transformation of steel at various weld thermal cycle. The basic requirement for good weldability of steels is to design the welding procedure to avoid the formation of large amounts of hard phase martensite in the HAZ of weld joint. In HSLA steel the preheating is beneficial to controlling the cooling rate of weld to reduce or avoid martensite formation in the HAZ. Preheat and interpass temperature depend upon the CE of the steel. By controlling the microstructure of the weld we can improve the toughness property of the steel.

$$CE = \%C + \frac{\%Mn}{6} + \frac{(\%Cr + \%Mo + \%V)}{5} + \frac{(\%Si + \%Ni + \%Cu)}{15}$$

The steel is considered to be weldable if CE is less than 0.40, If it exceeds from 0.40 susceptibility of weld under cracking from hydrogen embrittlement increases.

2.7 Effect of microstructure on fracture toughness

The microstructure is very much important to for the toughness properties of the steel. The both the transition temperature and toughness value is depend on the type of microstructure. The major microstructure constituents in the steel are, ferrite displays the highest transition temperature, followed by pearlite, upper bainite and finally lower bainite and tempered martensite. The transition temperature of each of constituent varies with temperature at which the constituent formed and, where applicable, temperature at which steel was tempered. the effect of different microstructure in steel are listed below.

2.7.1 Grain size

Grain size control is the most effective mechanism to control the toughness properties and strength of steel.

2.7.2 Ferrite

The fine grain acicular ferrite structure is desirable to increase the toughness of HSLA steel. Control rolling process promotes the formation of fine grain ferrite structure by preventing the recrystalisation of austenitic grains. Acicular ferrite is desirable from toughness point of view, and in the case of welding the of HSLA steel heat treatment and flux composition control in such a manner that promote the formation ferrite structure.

2.7.3 Pearlite

In strength point of pearlite is desirable but it detoriate the transition property, this leads to brittle fracture of the material. So it is desirable to control the pearlite concentration in the steel for toughness point of view at low temperature. It is due to increase in carbon with pearlite concentration.

2.7.4 Martensite

Martensites in steel are two types i.e. lath and twinned. The low carbon steel the lath martensite is formed. But if twinned martensite is formed in steel by any how, it decreases the K_{Ic} value by brittleness.

2.7.5 Bainite & tempered martensite

Isothermally transformed lower bainite has superior toughness, and slight lower transition temperature than tempered martensite of the same strength. However mixed structure which result from incomplete bainitic treatments causing partial transformation to martensite, have lower fracture toughness and much higher transition temperature than either 100% tempered martensite or 100 % lower bainite. Also upper bainite has higher transition temperature than lower bainite [16]. It is due to coarse interlathe carbides and common cleavage plane of the parallel ferrite crystal in packets of upper bainite.

The effect of microstructure on fracture mechanics of 1.6 % Cu strengthen HSLA-100 steel are available in literature [17]. The different microstructures are obtained by aging at different temperature of water quenched steel. The acicular ferrite and lath martensite structure has brittle fracture, but when lath martensite gets tempered, formation of polygonal ferrite and loss of coherency of Cu precipitates improved the toughness property. Finally the asymptotic rise in fracture toughness at the aging of $700^0 C$ is due to formation of reverted austenite and new martensite islands and growth of incoherent Cu precipitates. The martensite-austenite combination effectively acts as local composite entity and toughens the material by resisting easy propagation of cracks.

2.8 Stretch Zone Width, SZW

The length of crack extension that occurs during crack-tip blunting, for example, prior to the onset of unstable brittle crack extension, pop-in, or slow stable crack extension. The SZW is in the same plane as the original (unloaded) fatigue precrack and refers to an extension beyond the original crack size. Fracture behaviour of ductile materials is usually characterized by elastic-plastic fracture parameters such as the *J*-integral, stretch zone width, crack tip opening displacement etc .

In ductile materials, fatigue precrack blunts on the application of load to accommodate plastic strains arising out of the local deformation processes at the crack tip. On continuation of loading, the blunting at the crack tip increases and reaches a limiting size, governed by the deformation capacity of the material, and further initiates a fracture (ductile crack) at its tip. On a ductile fracture surface, crack tip blunting is manifested as a featureless region known as the stretch zone. The stretch zone that forms during the process of ductile fracture can be thought of as a frozen imprint of the state of deformation at the instant of the critical event of

ductile crack extension. Its extent can thus be used as a marker to indicate the corresponding fracture toughness parameter from the experimental resistance curve [18].

There is an intimate relationship between the fracture behavior of materials and the extent of the plasticity that occurs at the tip of the crack. There is experimental evidence that this crack-tip plasticity manifests itself as a stretch zone (SZ) ahead of the crack, the extent of which has been related to the fracture toughness. Of the fracture- toughness parameters used currently, the J-integral, represents the strength of the crack-tip singularity of elastic-plastic bodies, the value of being independent of geometry. The stretch zone during elasticplastic fracture is considered as a result of crack-tip blunting and can be correlated reasonably with the critical crack-tip opening displacement, which implies that the dimensions of the stretch zone can be a measure of the CTOD at fracture and are related directly to the fracture-toughness parameter, J_{IC} [19].

The procedure for using scanning electron microscopy for observation of the stretch zone is well documented [20]. The stretch-zone approach has been shown to be very useful for characterizing the fracture toughness of materials for which compliance measurements and the detection of the onset of crack growth are difficult to achieve and where a permanent record that can be verified independently in various laboratories is needed

2.9 Work reviewed

Several centuries' earlier experiments performed by Leonardo de Vinci provided some clues as to the root cause of fracture. He measured the strength of iron wires and found that the strength varied inversely with wire length. These results implied that flaws in material controlled the strength; a longer wire corresponded to a larger sample volume and a higher probability of sampling a region containing flaw. These results were qualitative in nature.

A quantitative connection between fracture stress and flaw size came from the work of Griffith [4], which was published in 1920. He applied a stress analysis of an elliptical hole to the unstable propagation of a crack. Griffith invoked the first law of thermodynamics to formulate a fracture theory based on a simple energy balance. Griffith's model correctly predicted the relationship between strength and flaw size in glass specimens. Subsequent efforts to apply Griffith model to metals were unsuccessful. Since this model assumes the

work of fracture exclusively comes from the surface energy of material, the Griffith approach only applies only to ideally brittle solids

Then came the famous liberty ship incident during World War II. These ships were completely welded. There was large number of failures of these ships. Some of the ships broke into two parts. Investigation revealed the ship failures were combination of three factors: weld defects, stress concentration at some locations and poor material used. Once the reasons of failure were identified. Corrective actions were taken whine manufacturing these Liberty ships in future. However, it led to a more detailed fracture research program in US Naval Research Laboratory in Washington DC under the leadership of Dr. G.R. Irwin. The first major contribution of Irwin was to modify the Griffiths approach to metals by including the energy dissipated by local plastic flow. In 1956**,** Irwin [5] developed energy release rate concept, which is related to Griffith theory, but in a form, which is more useful to solve engineering problems. Afterwards, Irwin developed the equation of the stress and strain field around a crack in an infinite plate using the Westergaard stress function approach. This paved the way for the development of a new field, known as Fracture Mechanics. A number of successful applications of fracture mechanics bolstered the standing of this new field in the engineering community.

The original motivation for development of fracture mechanics was to be able to account for materials that fracture with limited plastic deformation- that is, at applied stress levels less than those producing net section yielding. The discipline was initially focused on linear elastic brittle behavior. But, with the successes that were achieved with LEFM, materials for which such an approximation would be invalid also became of interest. To address the integrity of components made of these type of ductile materials in the presence of crack like defects, an alternative fracture mechanics model named as 'Elastic Plastic Fracture Mechanics' (EPFM) developed in late sixties and at later decades. Major thrust in the development of EPFM came in the late seventies and eighties when it was being extensively used to assess the integrity of piping of various nuclear power plants all over the world.

Rice [6] proposed a new parameter named J-integral, which has enjoyed great success as a fracture characterizing parameter for non-linear materials. By idealizing elastic –plastic deformation as nonlinear elastic, he provided the basis for extending fracture mechanics

methodology well beyond the validity of LEFM. Ductile tearing is normally controlled by micro void nucleation, growth, and coalescence mechanisms.

Tarfder, et al. [21] in their work, they have studied the ductile fracture behavior of primary heat transport piping material of nuclear reactor. In this paper, the fracture resistance of SA333, Grade 6 steel – the material used for Indian PHWR – under monotonic and cyclic tearing loading has been documented. An attempt has also been made to understand the mechanism responsible for the high fracture toughness of the steel through determination of the effect of constraint on the fracture behaviour and fractographic observations. From *J –R* tests over a range of temperatures; it was observed that SA333 steel exhibits embrittlement tendencies in the service temperature regime. The fracture resistance of the steel is inferior in the longitudinal direction with respect to the pipe geometry as compared to that in the circumferential direction. Imposition of cyclic unloading during ductile fracture tests for simulation of response to seismic activities results in a dramatic decrease of fracture resistance. It appears, from the observations of effects of constraint on fracture toughness and fractographic examinations, that fracture resistance of the steel is derived partly from the inability of voids to initiate and grow due to a loss of constraint in the crack-tip stress field.

Chattopadhyay et al [22], In the present paper, limit load based general expressions functions are proposed. These expressions are validated by deriving the known functions of pipe with through wall circumferential crack under four point bending load. The general expressions are then used to derive the functions of elbow with through wall circumferential crack configurations under in-plane bending moment, for which no solutions are available in the literature. Finally, experiments have been carried out on 200mm NB (Nominal Bore) elbows with through wall circumferential crack under in-plane bending moment. The proposed new expressions for this geometry are used to obtain the *J-R* curve from the experimental load vs. load line- displacement and load vs. crack growth data.

Chattopadhyay et al [23**],** Component Integrity Test Program was initiated in 1998 at Reactor Safety Division (RSD) of Bhabha Atomic Research Centre (BARC), India in collaboration with MPA, Stuttgart, Germany through Indo-German bilateral project. In this program, both theoretical and experimental investigations were undertaken to address various issues related to the integrity assessment of pipes and elbows. The important results of the program are

presented in this two-part paper. In the part II of the paper, the experimental investigations are discussed.

Part I covered the theoretical investigations. Under the experimental investigations, fracture mechanics tests have been conducted on pipes and elbows of 200–400 mm diameter with various crack configurations and sizes under different loading conditions. Tests on small tensile and three point bend specimens, machined from the tested pipes, have also been done to evaluate the actual stress–strain and fracture resistance properties of pipe/elbow material. The load– deflection curve and crack initiation loads predicted by non-linear finite element analysis matched well with the experimental results. The theoretical collapse moments of through wall circumferentially cracked elbows, predicted by the recently developed equations, are found to be closer to the test data compared to the other existing equations. The role of stress triaxialities ahead of crack tip is also shown in the transferability of J–resistance curve from specimen to component.

Chattopadhyay et al [24], In their work a number of fracture tests have been carried out on elbows with through wall circumferential/axial cracks subjected to in-plane closing/opening bending moment. These test data are then thoroughly analyses numerically through non-linear finite element analyses, analytically through limit load comparison and also through comparison of crack initiation loads by finite element and R6 methods. These test data may be utilized in future for validation of new theoretical developments in the integrity assessment of through wall cracked elbows.

E1-Fadaly et al [1], In their work number of Fracture mechanics tests, in addition to complementary mechanical tests, were carried out on 20MnMoNi55 steel, in the 0% pre-strain base-material as-rolled state and in the pre-strained $\pm 10\%$ states. All tests were carried out using 35 mm thick rolled plate of quenched and tempered 20MnMoNi55 steel (base material) having the chemical composition given in Table 1. The material selected is pre-strained uniaxially at room temperature, to two different values: +10% and -10%. Three groups of tests were then performed over a wide range of temperatures, from $-140^0 C$ to $400^0 C$, namely: tension, impact, and fracture tests .

The fracture mechanics tests were carried out on compact tension specimen (ICT) produced according to ASTM E813 [25], of 25 mm thickness (B) and 50 mm width (W). The

specimens were fatigue pre-cracked at room temperature according to ASTM E399 [26] to an initial crack length (a) given by *a/w* = 0.5. The fracture tests were carried out under displacement control using servo-hydraulic testing machines of 100 and 400 KN rated capacity, at a constant ram displacement rate of 0.4 mm/min. Three different techniques were used to determine the onset of stable crack extension, these being: the multispecimen technique , the single specimen technique [27] ; and the direct current potential drop technique (DCPD). During each test, a record of the load versus load-line displacement was obtained. Also, the J_i-value decreases with the pre-deformation: the J_i-value was found to be about $390\,N/mm^2$ for the base material, for the $218\,N/mm^2$ + 10% pre-deformation metal and about $167\,N/mm^2$ for the -10% pre-deformation metal. On the other hand, using the multi-specimen technique, the $J-\Delta a$ curves were determined for the base material and the - 10% pre-deformed metal, at room temperature with *a/w* ratio of 0.5, 0.6 and 0.7, to study the effect of the initial crack length on the J_{IC} value.. The J_{IC} has a value of $480\,N/mm^2$ in the case of *a/w* =0.5 and 0.7 and $430\,N/mm^2$ in the case of *a/w* = 0.6. At the strain rate of 1.38 × 10 -4 s -i, dynamic strain ageing takes place in the temperature range from 150 to 300°C for the base material and the + 10% pre-deformed metal. As compared with the base material, pre-deformation, whether positive or negative, causes an increase in the yield and ultimate tensile strength and a decrease in the elongation to fracture

Blauel et al [28] J-R curves have been determined for one specific forging of the reactor pressure vessel steel 20MnMo Ni55 to characterize its fracture resistance in the upper shelf toughness regime. The multiple specimen unloading (MSU), a direct current potential drop (DCPD), and the single specimen partial unloading compliance (SSP UC) methods have been applied to test different CT-specimen geometries at temperatures between 25 and 300 ° C. The *J-R* curves of 20MnMoNi55 are temperature dependent, showing a decrease in slope and absolute value for temperatures between 80 and 200°C and a re-increase for 300°C. The critical J-values for onset of stable crack growth in the scatter of the results are independent of temperature and geometry $J_i = 180\,KJ/m^2$. The values of the technical initiation toughness J_{IC} according to ASTM E813 [29] and according to Loss et al. (1979), the tearing modulus T, and the instability parameter. The material data have been used to evaluate the ductile failure initiation and tearing instability of several structural tests. The quality of agreement

between calculable predictions and experiments is shown to depend on the input material J-R curve and evaluation of the loading which requires detailed knowledge about the material stress-strain behaviour and the relevant crack tip constraint.

Singh et al [30] **,** in their work they have reported the tensile and fracture properties of SA333 Gr.6 carbon steel material which is used for the primary heat transport (PHT) system piping of the Indian pressurized heavy water reactor (PHWR). Tensile and J integral tests have been carried out on specimens machined from the base material as well as weldments of actual PHT pipes.

The SA333 Gr.6 carbon steel pipe (size 16 NB) with circumferential weld used in the primary heat transport system piping of 220 MWe Kaiga PHWR has been taken for preparing test specimens. The ASTM standard E813 [31] and El152 have been followed for testing. The single specimen technique has been used for J-R curve determination [32]**.** The specimens have been pre-cracked up to a crack length-to-width ratio (a/W) of 0.5 on an INSTRON 8501 servo-hydraulic testing machine using software controlled ΔK decreasing. Test procedure. The ΔK at the end of pre-cracking has been maintained 12- 15 $MPa\sqrt{m}$. Tests have been conducted at 28°C, 200°C, 250°C and 300°C. At each temperature, tests have been carried out with plain sided as well as side grooved specimens. He has observed that there is drop in the J-R curve at 288°C as compared to that at room temperature for SA333 Gr.6 steel. Kim et al. have made similar observation for SA106 Gr.C piping steel. Mukherjee et al [33], and Kim et al [34]. have also observed that the J-R curve at 288°C drops in comparison to 121°C for SA106 Gr.B and A516 Gr.70 steel. Yoshida et al have also reported the lowering of the J-R curve at higher temperatures for both base as well as weld metal of equivalent SA106 Gr.C steel. The material shows loss of ductility and tendency towards embrittlement at 250°C. The percentage loss in ductility is more substantial for the weld material than the base material; the J resistances of both base and weld materials decrease with increase in test temperature in general. But this decrease becomes pronounced at temperatures around 250°C. The J-resistance value of the weld metal at 250^0C is approximately 50% of that at room temperature for crack extension of 5 mm; fracture initiation toughness, J_i and $J_{0.2}$, decrease with increase in test temperature in general for base as well as weld metal; fracture resistance of base metal in L-C orientation has been observed to be higher than that of C-L orientation. The difference is more pronounced at higher temperatures.

Chen et al [35] For 10 mm thick smooth-sided compact tension specimens made of pressure vessel steel 20MnMoNi55, the interrelations between the cohesive zone parameters (the cohesive strength, T_{max}, and the separation energy, Γ) and the crack tip triaxiality are investigated. The slant shear-lip fracture near the side-surfaces is modeled as a normal fracture along the symmetry plane of the specimen. The cohesive zone parameters are determined by fitting the simulated crack extensions to the experimental data of a multi-specimen test. It is found that for constant cohesive zone parameters, the simulated crack extension curves show a strong tunneling effect. For a good fit between simulated and experimental crack growth, both the cohesive strength and the separation energy near the side-surface should be considerably lower than near the midsection. When the same cohesive zone parameters are applied to the 3D model and a plane strain model, the stress triaxiality in the midsection of the 3D model is much lower, the von-Mises equivalent stress is distinctly higher, and the crack growth rate is significantly lower than in the plane strain model. Therefore, the specimen must be considered as a thin specimen. The stress triaxiality varies dramatically during the initial stages of crack growth, but varies only smoothly during the subsequent stable crack growth. In the midsection region, the decrease of the cohesive strength results in a decrease of the stress triaxiality, while the decrease of the separation energy results in an increase of the triaxiality.

Vareda et al [36**],** the low-cycle fatigue, monotonic and fracture toughness behaviour of E3949, a Cr–Mn–N austenitic stainless steel, used for drillcollar connections was studied. Low-cycle fatigue tests were carried out at room temperature under total strain control in the range of 0.40 to 1.50% using Companion Specimens Test (CST) and Incremental Step Test (IST) methods. Cyclic softening without saturation was observed in all tests. Massing cyclic stress–strain behaviour was observed only with the IST method. The fatigue life behaviour obeyed Basquin and Coffin–Manson relationships and the high value obtained for ε'_f imparts a significant improvement in fatigue resistance of this alloy compared to AISI 304LN. The *J*–*R* curves and J_{IC} values were obtained at room temperature and at 150°C by using single specimens and the elastic compliance technique for crack length measurement. The observed decrease in crack initiation fracture toughness at 150°C is proposed to be due to a dynamic strain ageing effect, which impairs ductility. At room temperature, *J*IC values ranged widely from 97 to 155 kJ/m2. This variation can be attributed to microstructural inhomogeneities of the material. The decrease in crack initiation in fracture toughness at a temperature of 150°C is believed to be due to dynamic strain ageing effect, which impairs ductility. The strength

parameters and total elongation of E3949 steel decreased significantly with temperature, even at 100°C. Only reduction of area values showed an increase with temperature, but the increase was small, and then began to decrease slightly above 150.

Mogami et al [37] **,** Crack-growth behavior and tearing-instability characteristics under cyclic high stress were studied. The materials used in this study were STS42 carbon steel and A508 class 3 low-alloy steel. Tests were performed under both load-and displacement-control conditions. For a tearing-instability test, a high-compliance test apparatus was used. The cyclic J–R curve under lower initial **J** levels than J_{IC} showed lower values than a monotonic J–R curve. A wide range of fatigue-crack growth rates ($da/dN = 3-1 \times 10^{-5}$ mm/cycle) can be evaluated by using the equation in which ΔJ and J_{max} are used. In a high-compliance load system, it was shown that the critical **J** value at tearing instability under cyclic loading is almost equal to the value of **J** at an instability value under monotonic loading

Nakajima et al [38] , The ductile fracture toughness behaviour in the C-L orientation of type 321 stainless steel pipe service-exposed at 723 to 823 K for ˜ 51 000 h (the used material) was characterized using the multiple-specimen *J-R* curve technique at 293, 573 and 773 K. and at two straining rates (load-line displacement speed of 0.1 and 0.001 mm/min) in air environment. The behaviour was compared with the same material but not exposed to elevated temperature during service (the comparative material). J_{IC} of the used material is lower than the comparative material. The degradation is significant at 293 K, i.e. 160 kJ/m^2 for the comparative and 106 kJ/m^2 for the used. At elevated temperature, J_{IC} has decreased at the low strain rate. At 773 K and at strain rate of 0.001 nun/min, J_{IC} of the used and the comparative are 69 and 79 kJ/m^2, respectively, while at strain rate of 0.1 mm/min, 129 and 152 kJ/m^2, respectively. The slope of the *R* curve $(dJ/da)_R$, is also compared between the used and the comparative materials. Metallographic and fractographic examinations revealed that the degradation in fracture properties of the used is associated with aging-induced precipitation, more delamination at 293 K and more intergranular fracture at 773 K and at a strain rate of 0.001 mm/min than the comparative material.

Sivaprasad et al [39] In this work, an attempt is made to model the ductile fracture behaviour of two Cu-strengthened high strength low alloy (HSLA) steels through the understanding of their deformation behaviour. The variations in deformation behavior are imparted by prior deformation of steels to various predetermined strains. The variations in parameters such as yield strength and true uniform elongation with prior deformation is studied and was found to

be analogous to that of initiation fracture toughness determined by independent method. A unique method is used to measure the crack tip deformation characterized by stretch zone depth measurements were found to vary in the same fashion as the experimental values. A semi empirical relation for obtaining ductile fracture toughness from basic deformation parameters is derived and model is demonstrated to estimate initiation ductile fracture toughness accurately.

E. Roos et al [40], the engineering assessment of precracked components is frequently carried out with the help of crack resistance curves on the basis of the J-integral. Nevertheless, there are severe uncertainties regarding the validity of the J-integral in the case of large plastic deformations and unloading processes due to crack growth. Numerical and theoretical derivations are used to examine the influence of large plastic deformations and stable crack growth on the calculation of the J-integral. Numerical investigations were carried out on the example of a CT 25-specimen made of 20MnMoNi55 by means of the finite-element method. The following methods of calculations were selected:

- Calculation of the specimen behaviour without consideration of the stable crack growth.
- Calculation of the specimen behaviour using a J- Δa -curve as crack growth law.
- Calculation of the specimen behaviour using a damage model ("local approach") to compute the crack growth.

The results of the calculation carried out on the bagis of the damage model makes it possible to carry out an assessment of the various methods for the experimental determination of the J-value.

Bruninghaus et.al [41] The key curve method according to Ernst et al. was applied for the determination of J,-curves. Steels with different yield strength and toughness were investigated. The method requires a calibration curve, which has to be determined for each material and specimen type. It was shown for CT-specimens that crack extensions calculated by the key curve method are in good agreement with those observed on the fracture surfaces. The J,-values determined coincided well with values derived from ‘stretched-zone’ measurements and the equation for the ‘blunting-line’. It was demonstrated that the key curve method can be applied even at high loading rates. 1 CT-25specimens were tested at ram speeds up to 4 m/s. First results of instrumented charpy impact tests showed that crack propagation can be monitored in charpy V-notch specimens, too. On the other hand, crack

initiation is difficult to detect in the latter case because of superimposed oscillations in the load signal.

Roy et al [42] This investigation is aimed to examine the monotonic and cyclic fracture behaviour of AISI 304LN stainless steel and its weldments, in order to assess their integrity under seismic loading conditions. The monotonic fracture resistance of the steel has been determined using standard *J*-integral technique; whereas the cyclic fracture resistance has been evaluated using periodic unloading to different extents fixed by predetermined *R*-ratio. Comparison of the fracture toughness values of the steel estimated under monotonic and cyclic loading indicates that the latter could be as low as one fifth of the former. The observed degradation in cyclic fracture resistance has been attributed to crack-tip re-sharpening during cyclic loading. There is significant decrease in fracture resistance of AISI 304LN stainless steel and its weldment under cyclic loading compared to that under monotonic loading condition. The minimum $J_{0.2}$ value obtained by cyclic *J* integral tests is almost one-fifth of that estimated under monotonic loading condition both for base metal and the weldments. Fracture toughness decreases with decrease in load ratio, *R*. However, the lower bound *J*-*R* curves for AISI 304LN stainless steel and its weldment correspond to approximately $R = -1$. Thereafter, with further lowering of *R*-value the fracture resistance increases marginally. Fractographic examinations of the broken samples of AISI 304LN stainless steel, after monotonic and cyclic fracture tests, reveal that the ductile crack extension through micro void coalescence gets considerably influenced by smearing and fissure formation under cyclic loading condition. The monotonic fracture resistance of weldments is approximately 50% lower than the base metal of AISI 304LN stainless steel.

CHAPTER:3

MATERIAL, EXPERIMENTAL DETAILS AND TESTING PROCEDURES

3.1 Material

The material studied is German steel, used in reactor pressure vessel of Indian PHWR and designated as 20MnMoNi55. The 20MnMoNi55 steel used in this investigation has received from Bhabha Atomic Research Centre, Mumbai, India. The steel was received in the form of rectangular block. These components operate in the temperature range of $23-300^0C$. The material employed in such critical applications need understanding of the fracture behaviour in its operating temperature range. The specimens were made from this block to determine the fracture toughness of the selected steel using J-integral analysis, to understand the fracture behaviour of the steel at elevated temperature vis-a-vis that at ambient temperature and also to determine its conventional mechanical properties like hardness, tensile test at ambient temperature, tensile test at 300^0C .

3.2. Chemical Analysis

A small piece (of dimension 25mm x 25mm x 5mm) was cut from the as received material and its opposite surfaces were made parallel by grinding. This sample was used for determining the chemical composition of the steel.The chemical composition of the steel thus obtained is given in Table 3.1.

Table 3.1 Chemical composition of the steel.

Elements	C	Mn	Si	S	Mo	Cr	Ni
Wt%	0.2	1.25	0.3	0.05	0.5	0.17	0.6

3.3 Microstructure

3.3.1. Metallographic Specimen Preparation

Small test coupons of approximately 10mm x 10mm x 10mm size were cut from the as received material for metallographic examinations. These specimens were first ground successively on silicon carbide abrasive papers having grit sizes between 80 and 1200. Next the specimens were successively polished on Texemet cloth either using diamond paste of particle sizes of 1μm and 0.25μm or using colloidal suspension of beta alumina having particle sizes of 0.25μm and 0.1μm. Samples for microstructural studies were etched with freshly prepared 2% nital solution.

3.3.2 Metallographic Examination

The polished and etched metallographic specimens were studied using an optical microscope (Union Versamet-2) as well as a SEM. These examinations were carried out in three directions (L-T, S-L, and S-T) at different magnifications and several representative microstructures of the specimens were recorded.

3.4 Hardness Evaluation

Hardness was evaluated in three directions L-T, S-L and S-T surfaces with the help of a Vickers Hardness Tester using a load of 20 kgf. The specimen surfaces used for hardness studies were polished following the procedure described in section 3.3.1 prior to hardness examination. At least five indentations were taken to estimate the average value of hardness of the steel under investigation.

3.5 Tensile Testing

Round specimens of diameter 5mm and gauge length 25mm were fabricated for tensile tests following the ASTM standard E8 [43] from the as received block . The nominal dimensions of the tensile specimens are shown in Fig.3.1. Specimens were fabricated for evaluating tensile properties. All tests were carried out at a cross-head velocity of 0.003 mm/sec. The tests were conducted at room temperature and as well as at 300^{o}C. The tensile data were analyzed to estimate the yield strength (YS), ultimate tensile strength (UTS), uniform elongation (e_u), total elongation (e_t) and reduction in area.

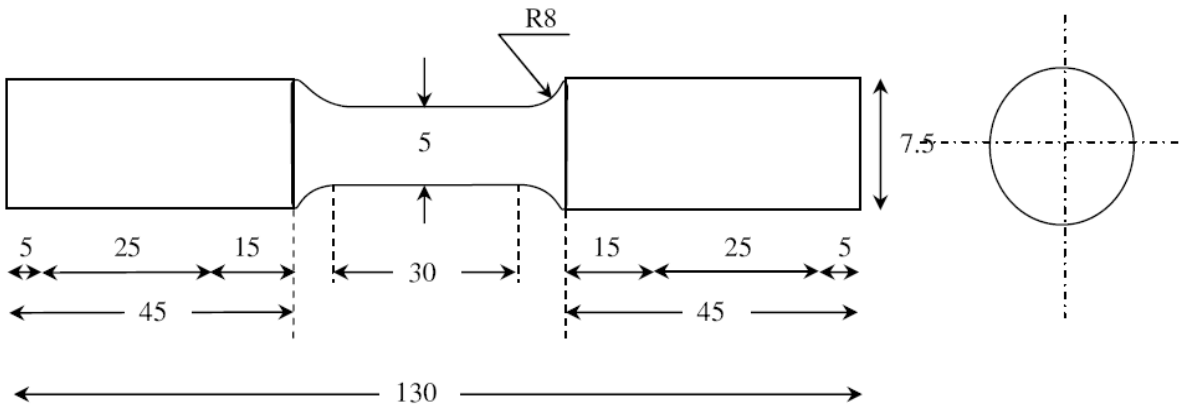

Figure 3.1: Typical round tensile test specimen

All tensile tests were performed with the help of an INSTRON (model: 8862) servo electric testing system fitted with a 100kN capacity load cell. Windows based software supplied by INSTRON. The software has provision for controlling the test conditions like displacement rate, and data acquisition on load, displacement and strain in different channels. The strain was measured through an extensometer of 25mm gauge length, attached to the middle of the specimen length. About 2500~3000 data points of engineering stress, percentage strain and displacement were acquired in each test for post processing.

The elevated temperature tensile tests were carried out in a three zone split type furnace placed around the specimen. The temperature of the specimen was monitored by a thermocouple tied at the centre of the test specimen. All elevated temperature tests were made with a temperature control of $\pm 3^0 C$ for measurement of specimen. Owing to the non-availability of a high temperature extensometer the stain of the specimens (tested at $300^0 C$) were calculated from actuator displacement data. The set up for the specimen displacement measurement is shown in Fig.3.2. After tying the thermocouple to the specimen, the furnace was enclosed and it was powered-up to achieve the desired test temperature. All tests were carried out after stabilizing the test temperature for 20~30 minutes.

Figure.3.2 Set up for the displacement measurement of a elevated temperature tensile test specimen

3.6 J-Integral test

3.6.1 Specimen Preparation

The fracture toughness tests in this investigation were planned on compact tension specimens in L-T orientation. Considering the available form of the material, standard 1CT specimens were machined following the guidelines of ASTM E 399-90 [44], in orientation, LT of the crack plane. Typical configuration of a specimen is shown in Fig 3.3. The designed dimensions of the specimens were; thickness (B) = 20mm, width (W) = 50mm and machine notch length (a_N) = 7.5mm. The dimensions of the specimens used in this investigation are shown in Table 3.2.

Fatigue pre-cracking of the CT specimens was carried out at room temperature in constant ΔK mode as described in ASTM standard E 647 [45] on servo hydraulic INSTRON testing machine using a commercial software (Advanced Fatigue Crack Propagation, AFCP) supplied by INSTRON Ltd U.K. The crack lengths were measured by compliance technique using a COD gauge of 5mm guage length fitted on the load line of the specimen. The software permitted on-line monitoring of the crack length (a), stress intensity factor range (ΔK) and the crack growth rate per cycle, da/dN. All pre-cracking experiments were carried out at a stress ratio of R = 0.1 using a frequency of 10Hz and with a constant ΔK is 20MPa√m. All specimens were pre-cracked to achieve a total crack length of approximately 25mm, which corresponds to $a/W \approx 0.45\text{-}0.5$. The total crack lengths a_0 (including fatigue pre-crack) for each specimen are given in Table 3.2. The pre-cracked specimens were provided with a side groove of 20% of the specimen-thickness. The side grooving was carried out by keeping a notch angle of 60^0 to a depth of approximately 2.5mm on each side of the specimen. This was done to enhance the stress tri-axialty at the crack tip and to enhance confidence level in the post–test measurement of Δa by optical means. The net thickness (B_N) of all the specimens is also shown in Table 3.2.

.

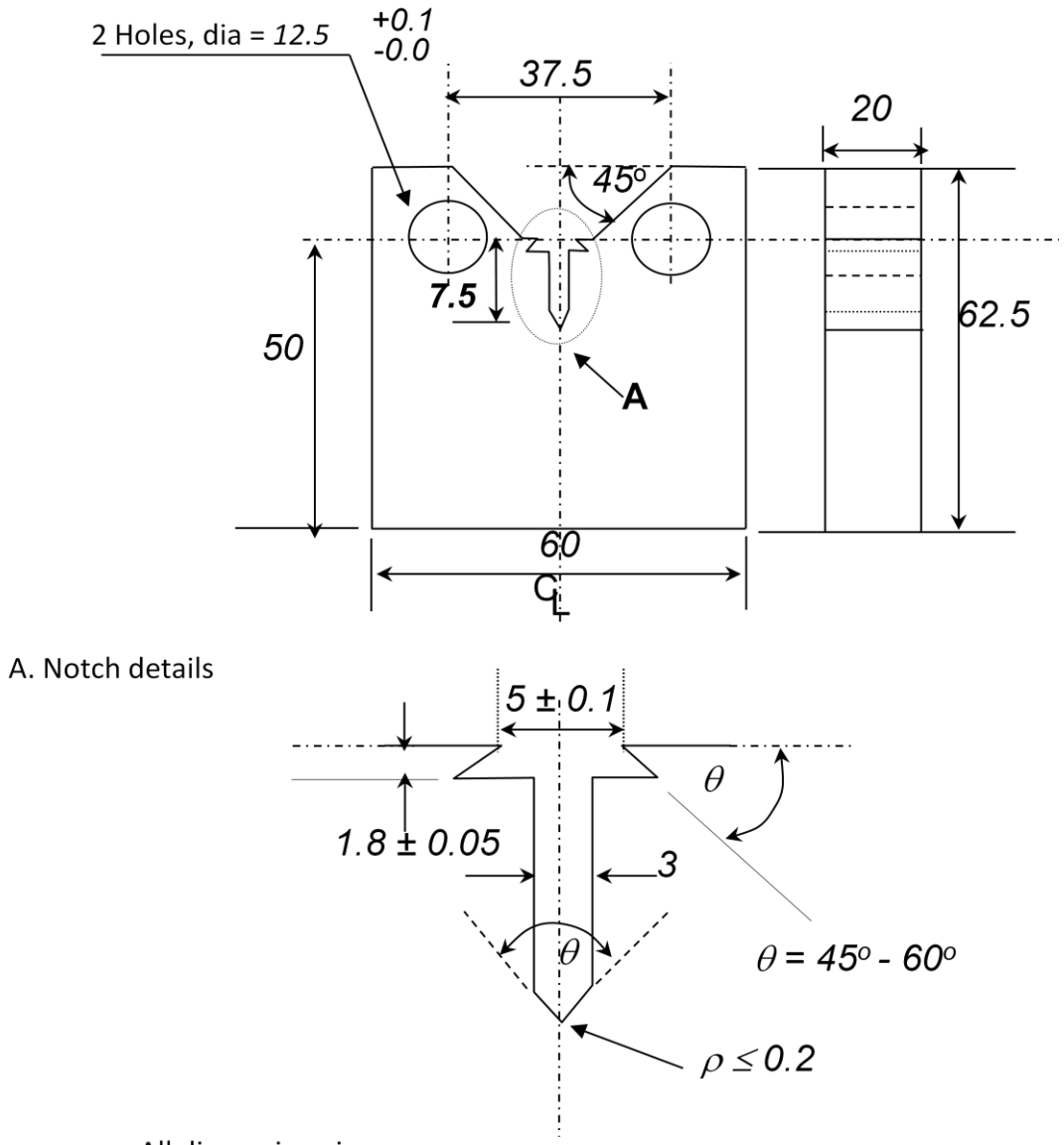

Figure. 3.3: Nominal Dimensions of 1CT Specimen

Table 3.2. Details of the tested CT-Specimens dimensions

Specimen code	Specimen dimensions			a_o (mm)	B_N (mm)
	W (mm)	B (mm)	a_N (mm)		
GM-01	49.70	19.96	7.63	18.12	15.94
GM-02	49.44	19.95	7.62	23.58	15.95
GM-03	49.76	19.93	7.70	25.89	16.09
GM-04	50.07	19.99	7.64	25.62	16.82
GM-05	50.01	19.96	7.74	24.19	16.64
GM-06	50.04	19.98	7.69	21.88	16.70
GM-07	50.05	20.06	7.78	18.20	16.70
GM-08	49.94	19.97	7.78	23.04	16.70
GM-09	50.03	20.01	7.70	27.76	16.72

W = width of the specimen,

B = total thickness of the specimen, B_N = net thickness of the specimen

a_N = machined notch length of the specimen, a_0 = crack length after pre-cracking,

3.6.2. Fracture Toughness Testing

The estimation of J-integral values of the fabricated specimens was carried out using an INSTRON (model: 8862) machine as described earlier (§ section 3.6.1). The single specimen unloading compliance technique has been used for evaluation of J-integral fracture toughness. In this method the crack lengths are determined from elastic unloading compliance measurements. This is done by carrying out a series of sequential unloading and reloading during the test, the interruptions being made in a manner that these are almost equally spaced along the load versus displacement record. These experiments have been carried out following the ASTM E 1820 [46] standard.

In the single specimen J-integral tests unloading should not exceed more than 50% of the current load value and hence design and control of the test procedure is important. Some initial trial experiments indicated that a specific actuator displacement control for the selected steel could lead to the desired test procedure. This control consisted of loading a specimen to a level of 0.3mm, unloading through 0.15mm, reloading through 0.15mm and then repeating the sequence till an appreciable load drop was noticed on the load displacement plot. A schematic representation of the variation of displacement with time used for the present tests is shown in Fig.3.4. The displacement cycles were carried out using an actuator rate of 0.003 mm s-1. The tests were controlled through a computer attached to the machine. The actuator displacement, load and the load line displacement (LLD), were recorded continuously throughout the test at a frequency of 2Hz. The magnitude of LLD was monitored by a crack opening displacement (COD) gauge of 10mm gauge length attached to the specimen. A minimum of approximately 35 data points of load-LLD was collected from the unloading part of the loading sequence for crack length calculations. A typical load displacement plot for a specimen tested at room temperature is shown in Fig.3.5 (a), 3.5(b).

The elevated temperature J-R- tests were carried out in an INSTRON split furnace. After mounting a CT specimen in its grips on the loading frame, the furnace was brought to position around the specimen, and was switched on. The loading on a specimen was started only after achieving the desired temperature and stabilizing it for 30 min. The temperature of the furnace was controlled by a three zone digital controller. A chromel-alumel thermocouple was tied on the specimen in a manner so that the temperature at the notch tip can be recorded. The temperature of the specimen during a test was monitored via this thermocouple. The J-R

tests were carried out at 300^0C temperatures in addition to the tests carried out at the ambient temperature of 28^0C.The setup for the J-R Test at 300^0C as shown in fig 3.6 a typical load displacement plot for a specimen tested at 300^0C temperature is shown in Fig.3.7 (a), 3.7(b).

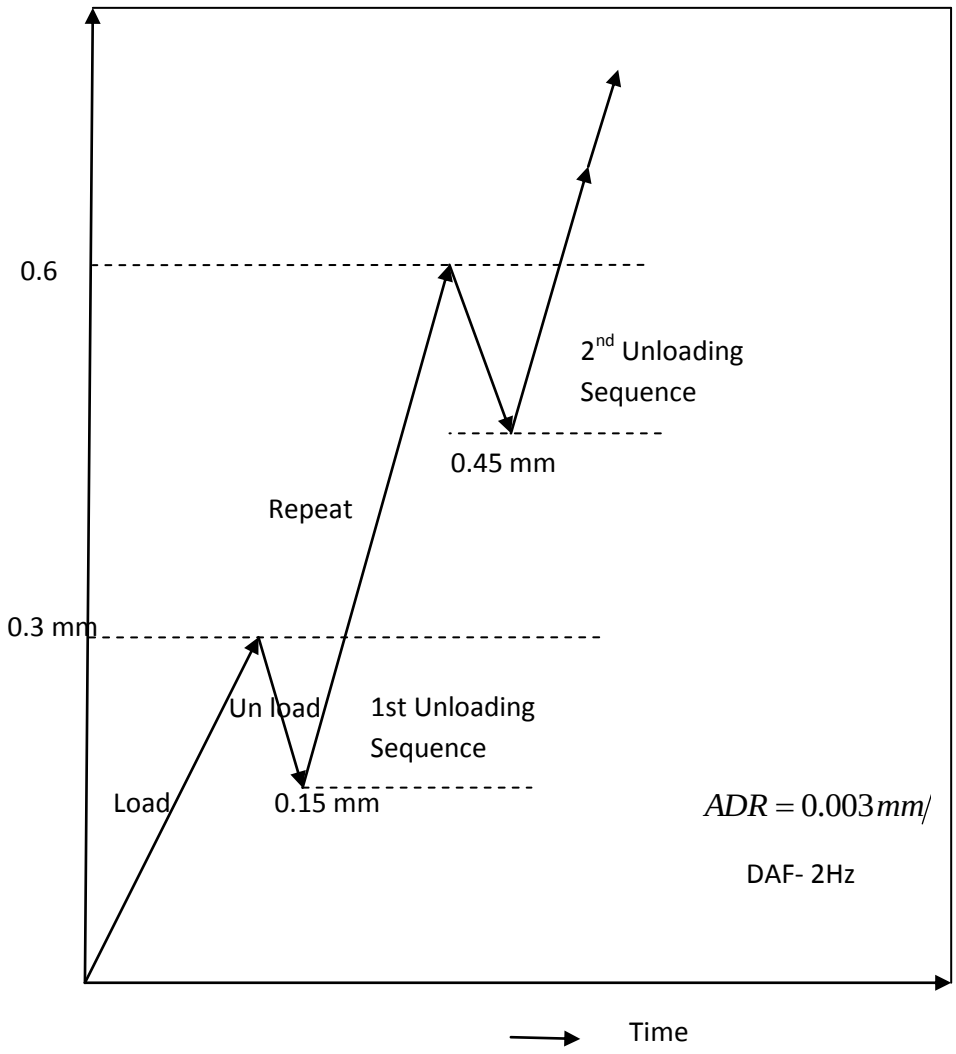

Figure.3.4. Schematic representation of the loading sequence for J-integral testing. The actuator displacement rate (ADR) and the data acquisition frequency (DAF) for these tests are also indicated.

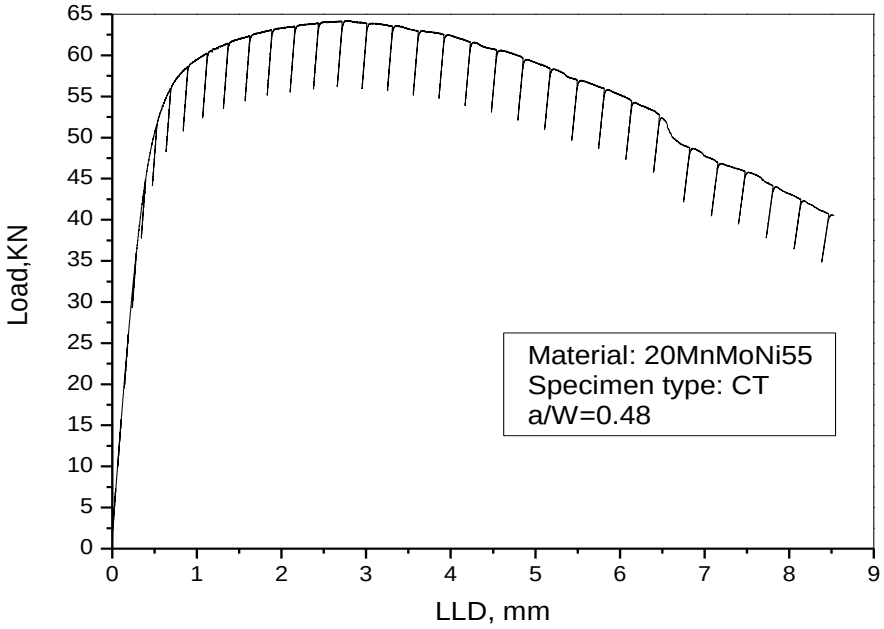

Figure.3.5 (a). Typical load vs displacement plot at 23^0C for GM-02 Specimen

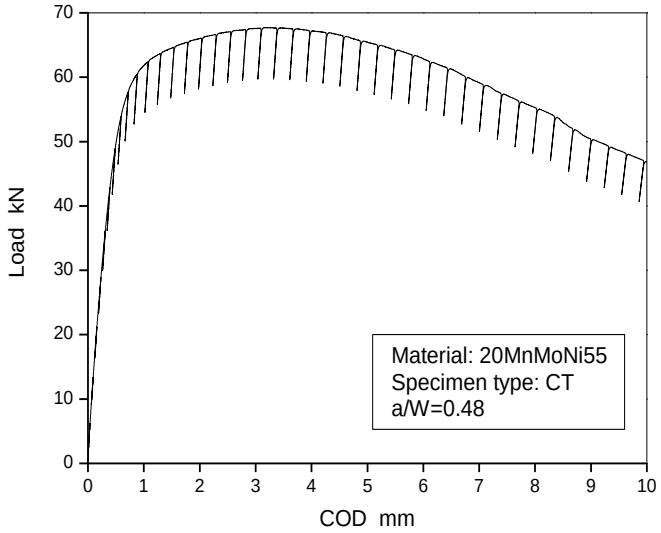

Figure: 3.5(b). Typical load vs displacement plot at 23^0C for GM-05 Specimen

Figure.3.6(a) Set up for the J- Test of CT- Specimen at $300^0 C$

Figure.3.6(b). Loading of CT specimen in J-Test

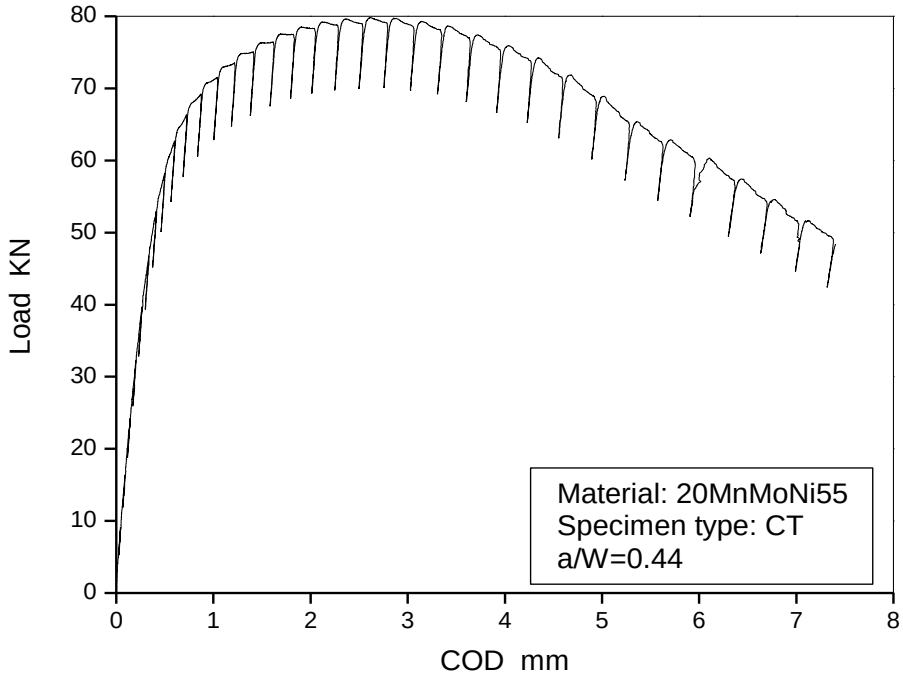

Figure.3.7 (a). Typical load vs displacement plot at 300 ^{0}C for GM-06 Specimen

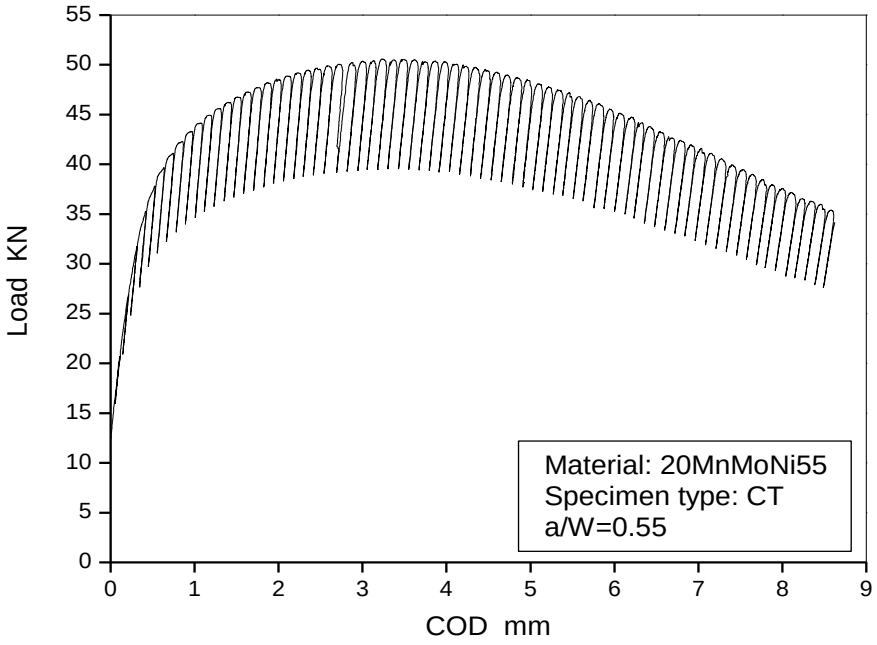

Figure.3.7 (b). Typical load vs displacement plot at 300 ^{0}C for GM-09 Specimen

The specimens, after the J-integral tests, were post fatigue cracked. The initial and the final crack lengths were measured as recommended in the ASTM standard [46] using a travelling microscope and these values were then compared with the crack lengths estimated through unloading compliance technique. The magnitudes of the optically measured crack lengths were found to be within ±0.05mm of that calculated by compliance crack length (CCL) relation as discussed next. This procedure was followed for all the tested specimens.

3.6.3 Generation of J-R curve

The experimental data obtained from the fracture toughness tests were analyses following the recommendations of ASTM standard E1820 [46]. The load vs. LLD data obtained from the tests were analysed to compute the magnitude of crack extension (Δa) and the corresponding J integral value at each unloading sequence.

The slope of each unloading path was calculated by linear regression analysis. The inverse of the slope yielded the compliance (C_i) of the specimen corresponding to the load from which the unloading has been carried out. The obtained C_i–values were corrected for the specimen rotation using the following expression to get the corrected compliance (C_{ci}) of the specimen at that particular load [45].

$$C_{ci} = \frac{C_i}{\left(\frac{H^*}{R}\sin\theta - \cos\theta\right)\left(\frac{D}{R}\sin\theta - \cos\theta\right)} \tag{3.1}$$

Where ,

H^* = initial half-span of the load points (centre of pin holes).

R = radius of rotation of the crack centre line, $(W+a)/2$, where a is the updated crack length

D = one half of the initial distance between the displacement measurement points

θ =angle of rotation of a rigid body element about the unbroken midsection line, or

$$\theta = \sin^{-1}\left[(d_m/2 + D)/\left(D^2 + R^2\right)^{1/2}\right] - \tan^{-1}(D/R) \tag{3.2}$$

d_m = Total measured load-line displacement.

The crack length (a_i) at this point of interest was next estimated using the expression suggested by Hudak et. al. [16] .

$$\frac{a_i}{W} = 1.000196 - 4.06319u + 11.24u^2 - 106.043u^3 + 464.335u^4 - 650.677u^5 \quad (3.3)$$

Where,

$$u = \frac{1}{(BEC_{ci})^{1/2} + 1} \quad (3.4)$$

$Be =$ Effective thickness of the specimen

$$= B - \left[\frac{(B - B_N)^2}{B}\right] \quad (3.5)$$

W =width of the specimen

B = total thickness of the specimen

B_N = Net thickness of the specimen

$$\Delta a = a_i - a_0 \quad (3.6)$$

The magnitude of J is the sum of its elastic and plastic component denoted by J_{el} and J_{pl}. The elastic component of J was calculated using the equation

$$J = J_{el} + J_{pl} \quad (3.7)$$

$$J_{el(i)} = \frac{(K_{(i)})^2(1 - \upsilon^2)}{E} \quad (3.8)$$

Where K_i is the elastic stress intensity parameter evaluated using the expression given below [18].

$$K_i = \left[\frac{P_i}{(BB_N W)^{1/2}}\right] f(a_i / W) \quad (3.9)$$

$$f(a_i/W)=\left[\frac{\left(2+\frac{a_i}{W}\right)\left(0.886+4.64\left(\frac{a_i}{W}\right)-13.32\left(\frac{a_i}{W}\right)^2+14.72\left(\frac{a_i}{W}\right)^3-5.6\left(\frac{a_i}{W}\right)^4\right)}{\left(1-\left(\frac{a_i}{W}\right)\right)^{3/2}}\right] \quad (3.10)$$

The magnitude of J_{pl} was calculated by considering only load vs plastic load line displacement. In order to obtain the latter, the elastic part of displacement at different loads was first calculated from the slope of the initial load-LLD diagram. A simple subtraction of the elastic component from the total displacement yielded the plastic part of LLD. The area under the load vs plastic LLD data from the start of the test to the load of interest was calculated to obtain the magnitude of J_{pl}. This was done by using the expression [46]:

$$J_{pl(i)}=\left[J_{pl(i-1)}+\left(\frac{\eta_{(i-1)}}{b_{(i-1)}}\right)\left(\frac{A_{pl(i)}-A_{pl(i-1)}}{B_N}\right)\left(1-\left(\gamma_{(i-1)}\right)\left(\frac{a_{(i)}-a_{(i-1)}}{b_{(i-1)}}\right)\right)\right] \quad (3.11)$$

Where ,

$$\eta_{(i-1)}=2.0+0.522b_{(i-1)}/W$$

$$\gamma_{(i-1)}=1.0+0.76.b_{(i-1)}/W$$

The quantity $A_{pl(i)}-A_{pl(i-1)}$ is the increment of plastic area under the force versus plastic load-line displacement record between lines of constant displacement at points i-1 and i. . The quantity $J_{pl(i)}$ represents the total crack growth corrected plastic J at point i and is obtained in two steps by first incrementing the existing $J_{pl(i-1)}$ and then by modifying the total accumulated result to account for the crack growth increment .Accurate evaluation of $J_{pl(i)}$ from the above relationship requires small and uniform crack growth increments and consistent with the suggested elastic compliance spacing .The quantity $A_{PL(i)}$ can be calculated from the following equation.

$$A_{pl(i)}=A_{pl(i-1)}+\left[\frac{(P_{(i)}+P_{(i-1)})(V_{pl(i)}-V_{pl(i-1)})}{2}\right] \quad (3.12)$$

Where ,

$V_{pl(i)}$ = plastic part of the load-line displacement, $V_{(i)}-\left(P_{(i)}C_{LL(i)}\right)$, and

$C_{LL(i)}$ = Experimental compliance, $(\Delta V / \Delta P)$, corresponding to the current crack size.

The obtained values of J and the corresponding crack extension Δa were plotted to get the J-Δa curves of the material in various test conditions.

3.6.4 Fractography

The end of the ductile crack extension during loading of the specimens, subjected to J-integral test, was marked by post fatigue cracking, and then the specimens were loaded to fracture. The fractured surfaces were ultrasonically cleaned and examined using a scanning electron microscope. This was done to record the interesting features of stable crack extension.

CHAPTER: 4

RESULTS AND DISCUSSIONS

4.1. INTRODUCTION

The integrity of the pressure vessels of nuclear power plants in which the selected steel is used is commonly assessed using Leak Before Break (LBB) concepts. The LBB approach using fracture mechanics principles attempts to ensure that no catastrophic rupture would occur in an engineering component without prior indication of detectable leakage. In order to encompass fracture mechanics principles in such component integrity program one requires information and understanding about the fracture behaviour of a material in different experimental conditions. This chapter deals with studies related to mechanical properties like microstructure, hardness, tensile properties at room temperature and elevated temperature and crack initiation toughness of the 20MnMoNi55 steel in monotonic loading condition

4.2 Discussion on Micro structure

The polished and etched metallographic specimens were studied using an optical microscope (Union Versamet-2) as well as a SEM. These examinations were carried out in three directions (L-T, S-L and S-T) at different magnifications and several representative microstructures of the specimens were recorded.

The typical microstructure of 20MnMoNi55 steel as shown in fig.4.1 this microstructure consists of Bainite and Ferrite phases.

Bainite is randomly oriented in ferrite matrix, which gives more toughness. The ferrite gives ductility and bainite gives strength to the investigated steel.

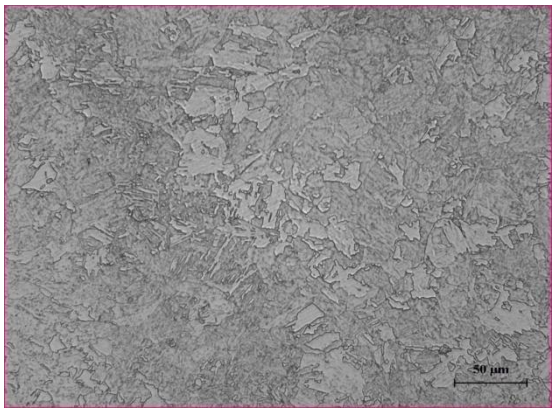

(a)

(b)

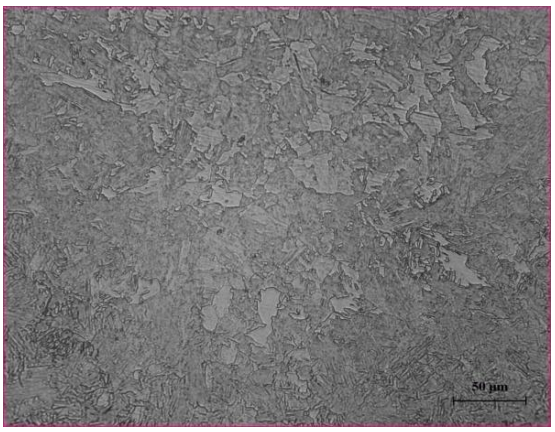

(c)

Figure: 4.1 Typical optical microstructures of the investigated steel in (a) L-T direction (b)S-L Direction (c) S-T Direction

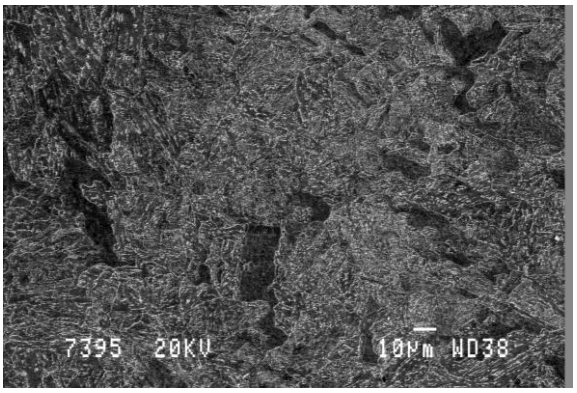

(a)

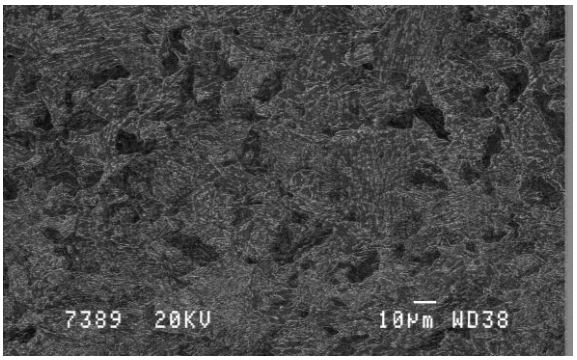

(b)

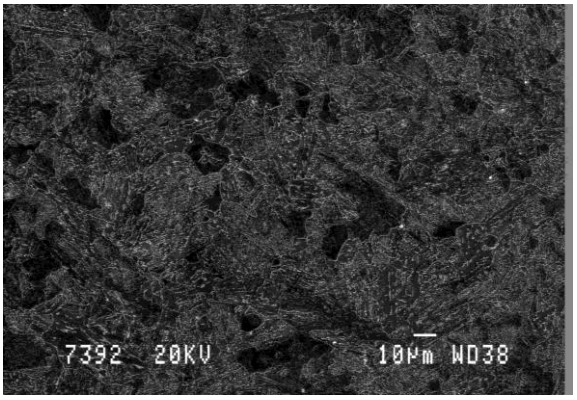

(c)

Figure .4.2 Typical SEM microstructures of the investigated steel (a) L-T direction, (b) S -L direction, (c) S-T direction

4.3 Discussion on hardness

Hardness was evaluated in three directions L-T, S-L and S-T surfaces with the help of a Vickers Hardness Tester using a load of 20 kgf as shown in table: 4.1. The five indentations were taken to estimate the average value of hardness of the steel under investigation.

Table .4.1. Hardness values of 20MnMoNi55 steel

Direction	Diameter of indentation (d) mm	Hardness HV
L-T	0.421	209
S-L	0.413	217
S-T	0.416	214

4.4 Tensile test

The tensile tests were conducted at room temperature and elevated temperatures. The stress strain plot at 28^0C is shown in Fig. (4.3) and the tensile properties in Table 1. The stress displacement plot at 300^0C is shown in fig (4.4) and tensile properties in Table 2.

Table .4.2: Tensile Properties of 20MnMoNi55 steel at Room Temperature

YS, MPa	UTS ,MPa	e_u (%)	e_t (%)	RA (%)	E MPa
490	620.5	9.51	23.01	68.65	210

Table .4.3: Tensile Properties of 20MnMoNi55 steel at 300^0C Temperature

YS MPa	UTS MPa
443	621

YS: Yield Strength, UTS: Ultimate Tensile Strength

e_u : Uniform elongation, e_t : Total elongation, RA: Reduction in Area

E : Elastic modulus

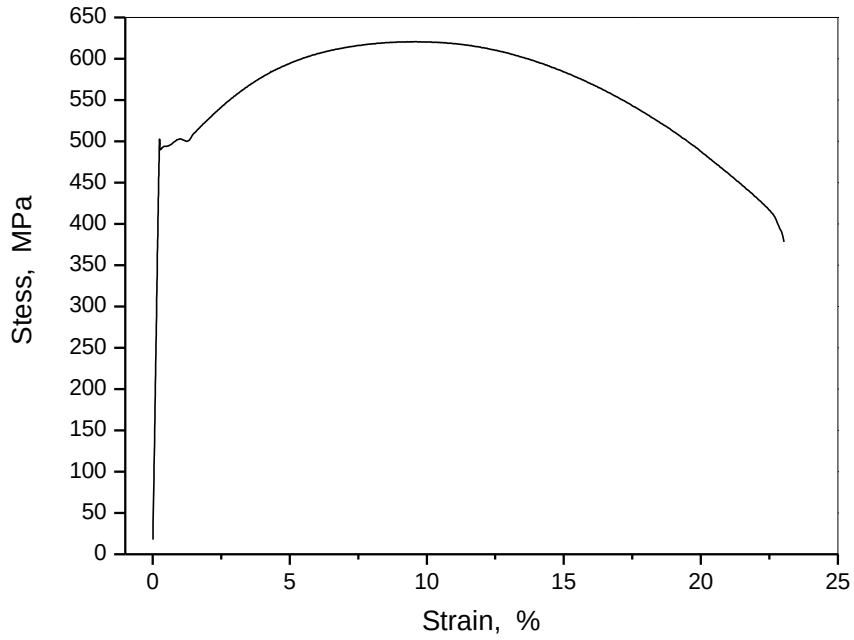

Figure.4.3. stress-strain behaviour of 20MnMoNi55 steel at Room Temperature

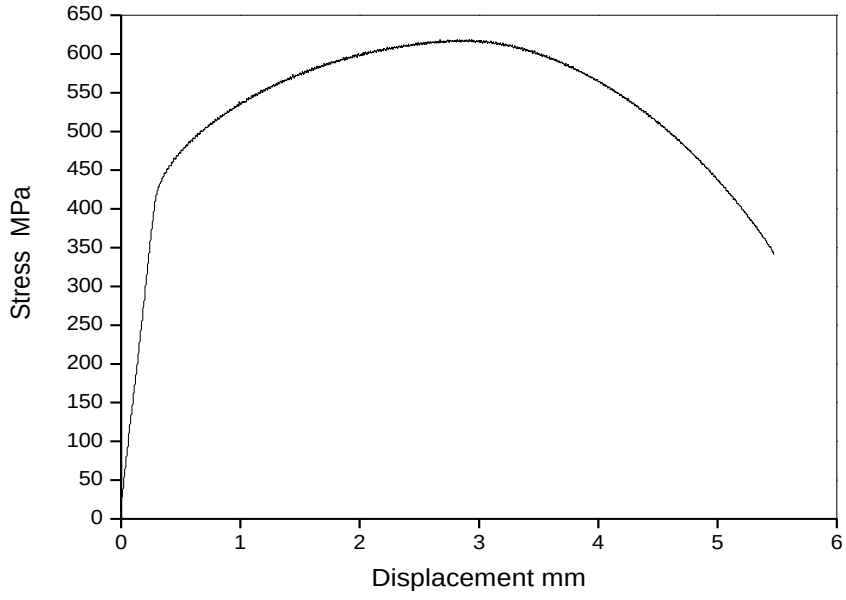

Figure.4.4. stress-Displacement behaviour of 20MnMoNi55 steel at $300^0 C$ Temperature

The room temperature engineering stress-strain diagram of the 20MnMoNi55 steel is shown in Fig.4.3.. The high temperature engineering stress-strain diagrams of the 20MnMoNi55 steel is shown in Fig.4.4. The room temperature tests showed distinct yield point where as high temperature tests do not show any yield point phenomenon. The yield strength of high temperature tests was obtained by 0.2% strain offset procedure, as these do not show clear yield point. The tensile parameters evaluated at room temperature and at 300^{o}C for 20MnMoNi55 steel material are summarized in Table 1 and Table 2 respectively.

All the room temperature tensile tests showed a distinct yield point phenomena followed by an inhomogeneous plastic deformation. However, such a phenomena was not observed during high temperature tensile deformation. Yield point phenomena occur due to dislocations being pinned down by interstial atoms. To knock out the dislocations from these obstacles higher stresses are required (occurrence of upper yield point). Once the applied stress is sufficient enough to release the dislocations from these obstacles, there will be a sudden drop in the applied stress (occurrence of lower yield point) as low stress is sufficient enough to cause further movement of dislocations. Upon knock out, the dislocations will move rapidly over a distance, causing an inhomogeneous deformation before coming in to interaction with other dislocations/obstacles to effect homogenous deformation of the material. This is exactly what happens during the room temperature tensile deformation of 20MnMoNi55 steels. However, during high temperature, the interstials, that are the main source of obstacles for the dislocations, will be in a state of constant motion. Therefore the chances of dislocations being locked up at the obstacles and thereby causing an yield point phenomena as in room temperature deformation are less. The material will therefore undergo homogenous plastic deformation right away at high temperatures.

4.5 J-integral Fracture toughness

In this section the procedure employed to evaluate the critical value of J is first presented. The estimated critical values of J are next discussed in two subsections elucidating the fracture behaviour of the material at ambient and at elevated temperatures. A typical J-R curve (a plot of J against Δa) at room temperature as shown in fig:4.5and fig:4.6. A typical J-R curve (a plot of J against Δa) at elevated temperature as shown in fig 4.7and fig: 4.8.

4.5.1 Determination of the Critical J-integral Fracture toughness

A typical J-R curve (a plot of J against Δa) for the specimen is shown in Fig.4.9. The *J-R* curve consists of a plot of *J* versus crack extension in the region of *J* controlled growth

Corrections and Adjustments to Data

In an elastic compliance method, a correction is applied to the estimated Δa_i data values to obtain an improved a_{oq}. This correction is intended to obtain the best value of a_{oq}, based on the initial set of crack size estimates a_i, data.

Adjustment of a_{oq}

The value of J_Q is very dependent on the a_{oq} used to calculate the Δa_i quantities.

Identify all J_i and a_i pairs that were determined before the specimen reached the maximum force for the test. Use this data set of points to calculate a revised a_{oq} from the following equation [45].

$$a = a_{oq} + \frac{J}{2\sigma_Y} + BJ^2 + CJ^3$$

The coefficients of this equation shall be found using a least squares fit procedure.

For each a_i value, calculate a corresponding Δa_i as follows:

$$\Delta a_i = a_i - a_{oq}$$

Determine a blunting line in accordance with the following equation

$$J = m.\sigma_0.\Delta a$$

Where, the value of m is taken as 2.

The parameter σ_0 is the flow stress of the material at the test temperature and was taken as $(\sigma_{YS} + \sigma_{UTS})/2$. The values of σ_{YS} and σ_{UTS} have been already reported in Table 4.2and

Table 4.3. The values of σ_{YS} and σ_{UTS} were taken from the results of tensile tests carried out at the actuator displacement rate 3x10-3mms-1. The ASTM blunting line for the specimen was computed and however, this line does not intersect the experimental J-R curve. Similar observations were also made further other tested specimens as listed in Table 4.4. These observations are in following the results reported by several earlier investigators on high toughness materials [1, 21, 28, 30]. In order to estimate the J_Q values, an experimental blunting line, was then drawn considering the initial linear portion of J vs. Δa data for each of the specimens. The slopes of such blunting lines were estimated, and the values of m were calculated from the slope values using the corresponding value of σ_0.

Then draw an exclusion line parallel to the construction line intersecting the abscissa at 0.15 mm. Draw a second exclusion line parallel to the construction line intersecting the abscissa at 1.5 mm. Plot all J - Δa data points that fall inside the area enclosed by these two parallel lines.

In order to fit the power law equation for J-R curve, the experimental points of J vs. Δa lying between two exclusion lines were considered. The exclusion lines were constructed parallel to the experimental blunting line at Δa-offset values of 0.15 and 1.5mm following the ASTM standard E-1820 [46]. The experimental points between the two exclusion lines were then fitted to a power law equation of the form [46]:

.

$$\ln J = \ln C_1 + C_2 \ln\left(\frac{\Delta a}{k}\right)$$

$$J = C_1(\Delta a)^{C_2}$$

Where C_1 and C_2 are material constants at the test conditions

A line parallel to the experimental blunting line at Δa = 0.2mm was next constructed. The intersection of this offset line with the fitted J-R curve was considered as the critical value of J, i.e. J_Q.

Then draw 0.2mm offset blunting line. The intersection of the blunting line with the power law curve at an offset of 0.2 mm was considered as J_Q . Determine J_i at intersection of blunting line with power law curve as shown in figure.4.9

The blunting line was re-constructed for the data points falling within the window of $0.2J_Q - 0.6J_Q$ and the entire procedure was iterated till the blunting line slope and the constants C1 and C2 converged.

Two typical evaluations of J_Q for specimens GM-05, GM-07 are shown in Fig.4.9 and Fig.4.10 respectively. Estimations of J_Q for the other specimens were also made in a similar manner. The results of J_Q and J_i are shown in Table 4.4. The estimated J_Q values were next examined for the validity of referring these as J_C / J_{IC} as per ASTM standard E1820 [46]. The validity criterion states the thickness (B) and the remaining ligament (b_0) of the specimen should be greater than $10(J_Q / \sigma_0)$. A typical calculation indicates the thickness requirement to be 17.73 mm for the specimen GM-05 considering J_Q = 983.97kJ/m2 and σ_0 = 555 MPa. This thickness is less than the thickness of the tested specimen and even that of the available maximum thickness of the block. Hence the evaluated J_Q value for this specimen can be referred as J_C / J_{IC} as per ASTM standard E1820 [45]. Similar results (Table 4.4) were obtained when the J_Q for the other specimens were subjected to the validity test. The J_Q values estimated in this investigation are considered as the critical fracture toughness criterion of the material, and are denoted as J_{IC} in further discussion.

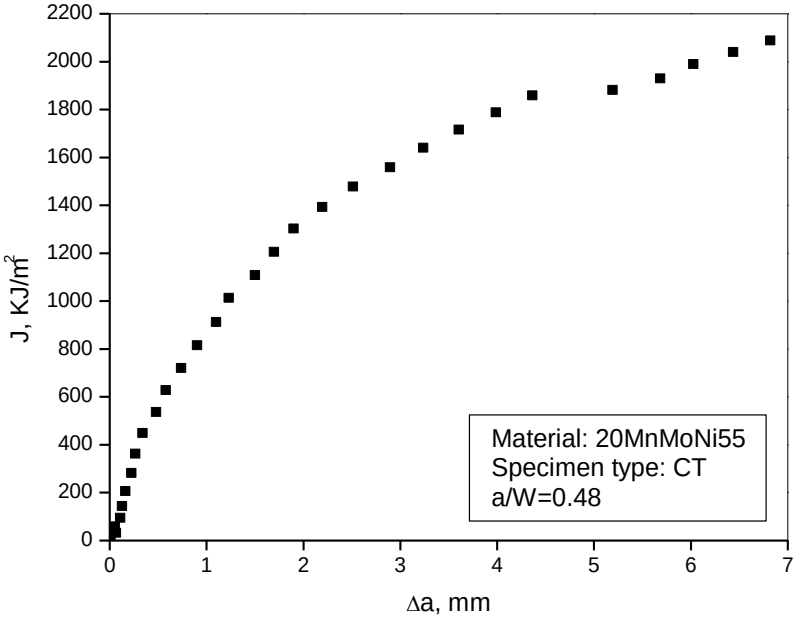

Figure. 4.5. Typical J-R curve for GM-02 Specimen at $23^0 C$

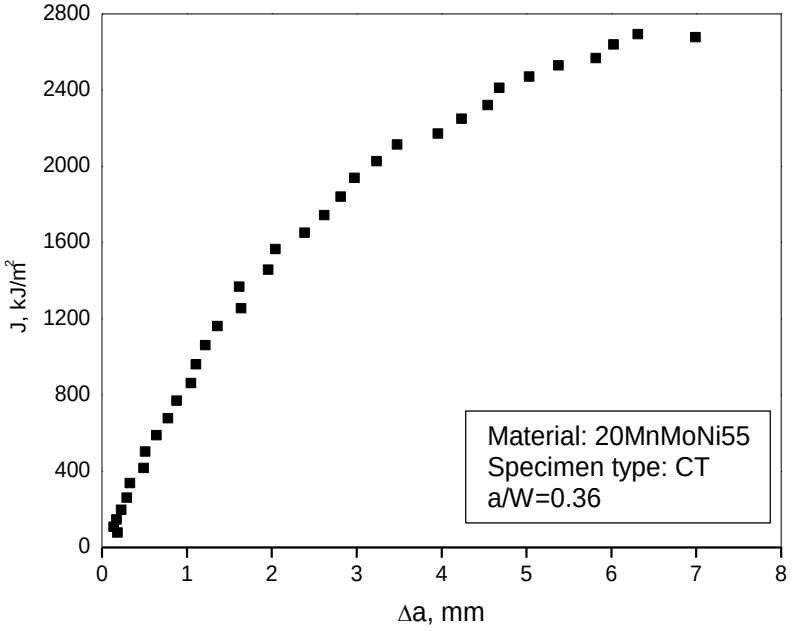

Figure. 4.6.Typical J-R curve for GM-05 Specimen at $23^0 C$

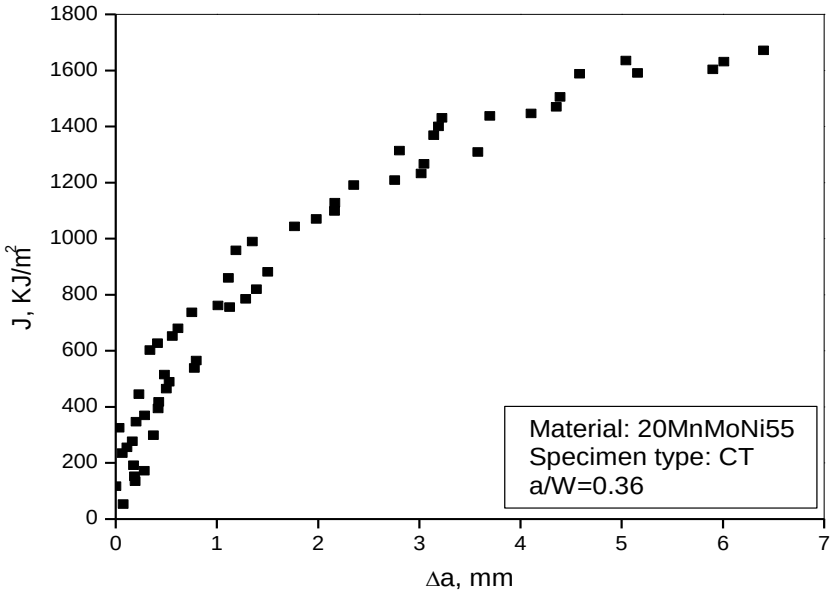

Figure. 4.7. Typical J-R curve for GM-07 Specimen at $300^0 C$

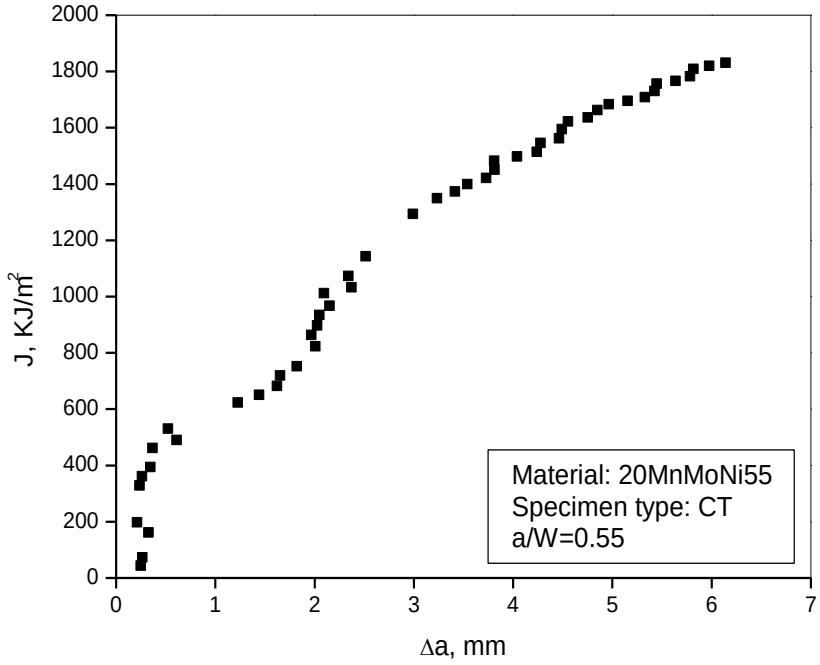

Figure. 4.8. Typical J-R curve for GM-09 Specimen at $300^0 C$

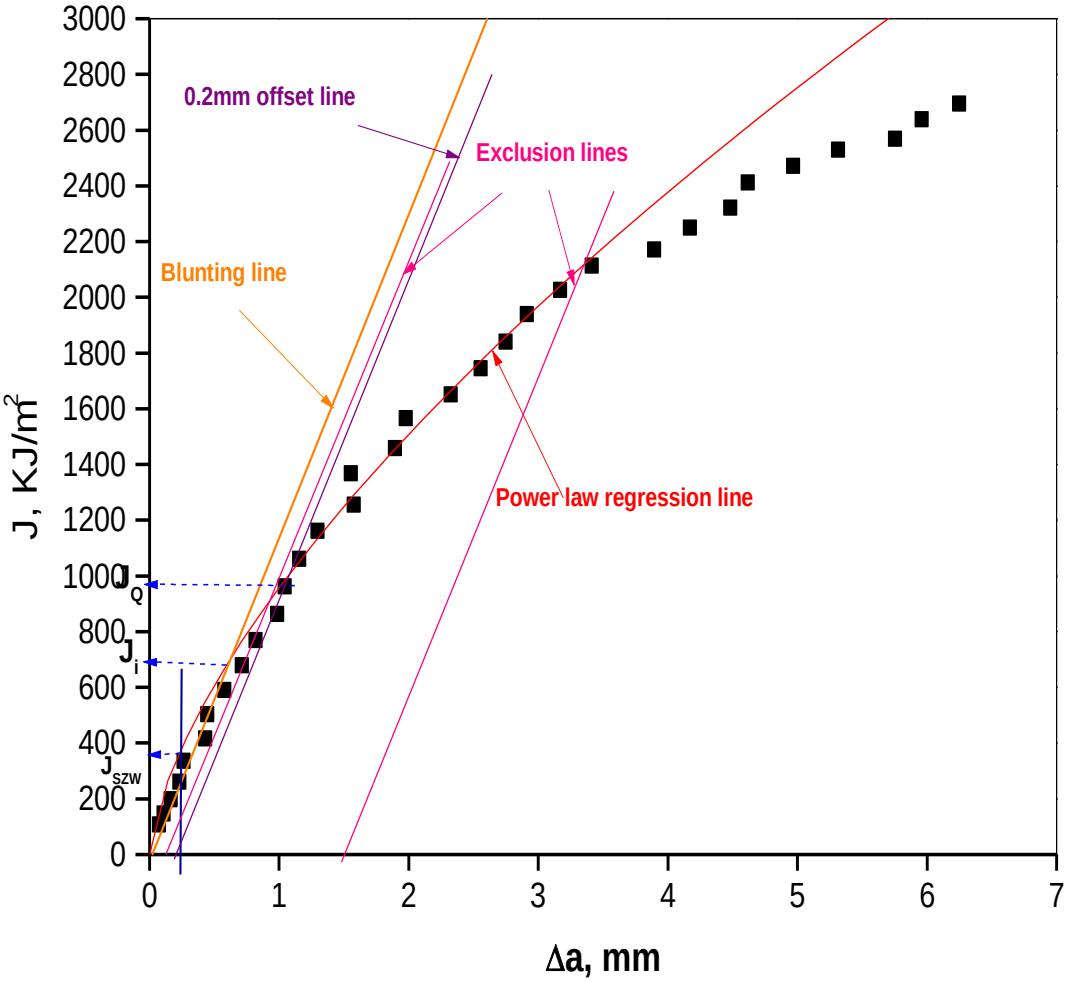

Figure.4.9. Typical J-R curve for GM-05 specimen at $23^0 C$

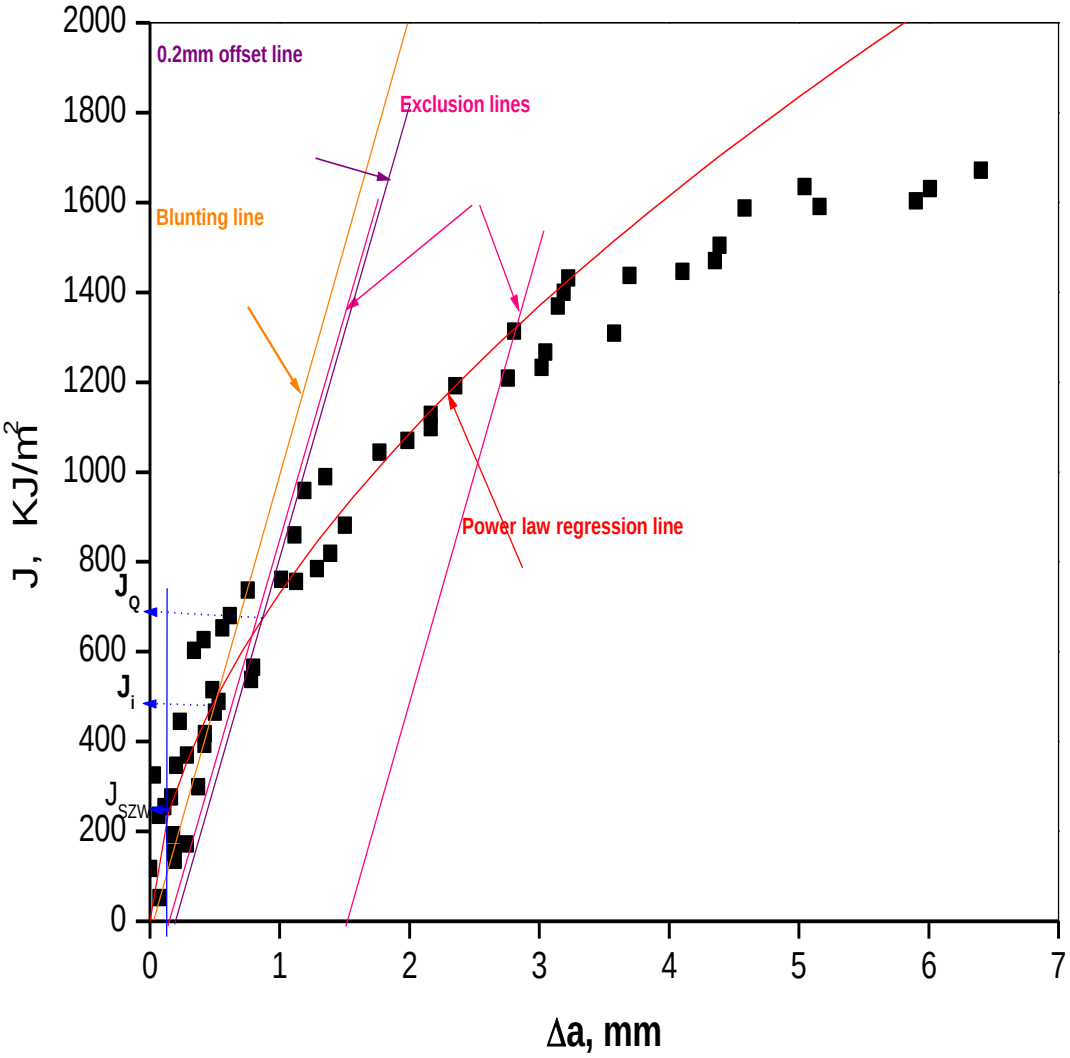

Figure. 4.10. J-R curve for GM-07 specimen at $300^0 C$

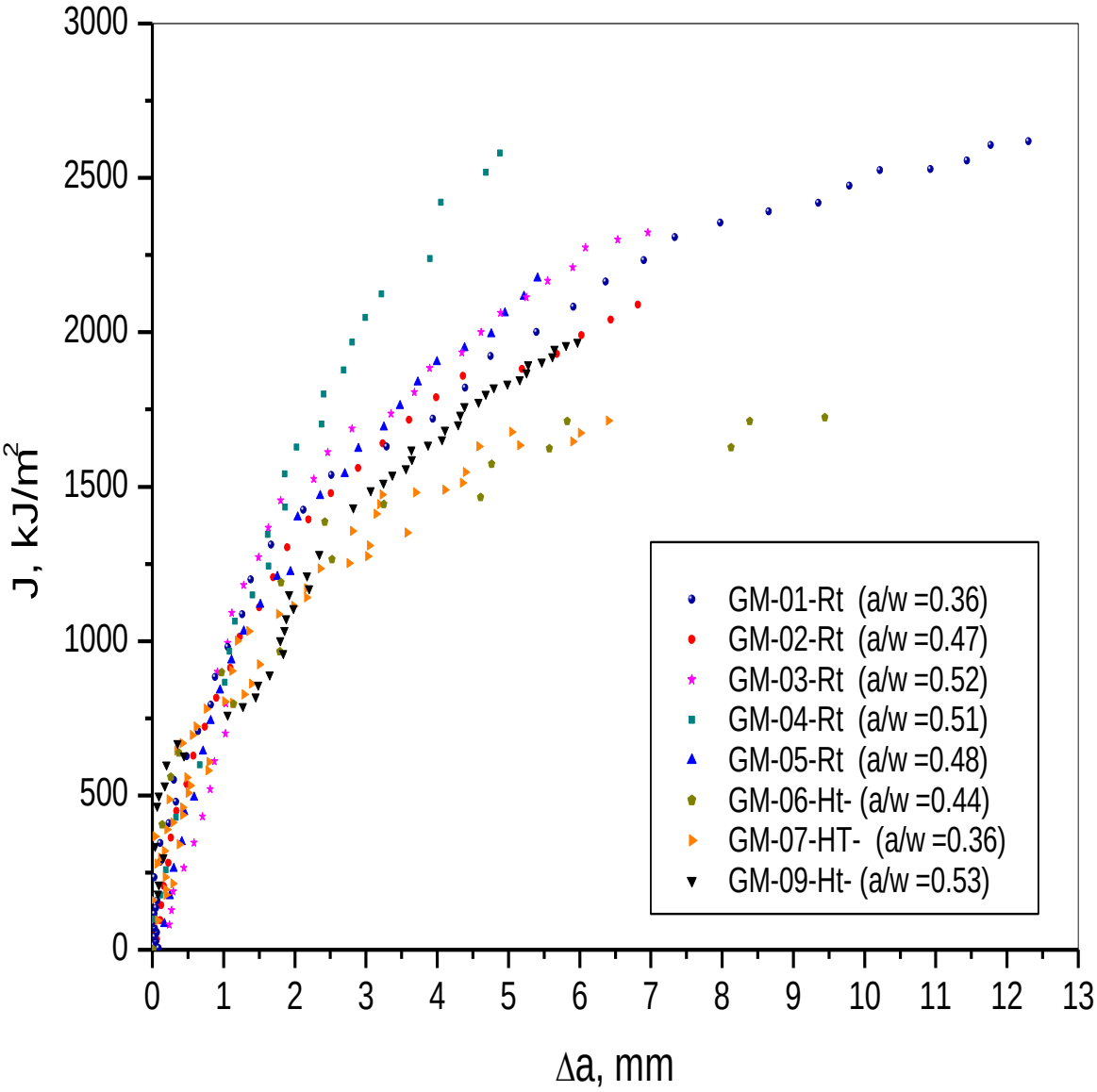

Figure.4.11. Comparison of room temperature and high temperature J-R curves

Table 4.4 Fracture toughness parameters of the investigated steel

Specimen code	Temp. ^0C	a_{oq} mm	a/W	J_Q KJ/m^2	J_i KJ/m^2
GM-01	23	18.01	0.36	602.08	273.72
GM-02	23	23.04	0.46	743.75	489.55
GM-03	23	25.93	0.52	1479.76	1411.80
GM-04	23	26.33	0.52	2032.18	1890.00
GM-05	23	24.52	0.48	983.97	677.82
GM-06	300	21.88	0.44	655.85	517.87
GM-07	300	17.23	0.34	670.12	479.87
GM-09	300	26.92	0.53	670.34	545.30

Table 4.5. Thickness validity criteria of the specimens for fracture toughness test

Specimen code	Temp. ^0C	σ_0 MPa	J_Q KJ/m^2	B (mm)	$10(J_Q/\sigma_0)$
GM-01	23	555	602.08	19.96	10.85
GM-02	23	555	743.75	19.95	13.40
GM-03	23	555	1479.76	19.93	26.67
GM-04	23	555	2032.18	19.99	36.614
GM-05	23	555	983.97	19.96	17.73
GM-06	300	582	655.85	19.98	11.27
GM-07	300	582	670.12	20.06	11.51
GM-09	300	582	670.34	20.01	10.85

σ_0 = flow stress, J_Q = critical value of J,

B = specimen thickness, and $10(J_Q/\sigma_0)$= thickness criterion.

4.5.2 J Integral Fracture Toughness at Room Temperature

The estimated average J-integral fracture toughness values of the steel at room temperature is 776.6 KJ/m^2 (§ Table 4.4) for specimens GM-01, GM-02 and GM-05. M.S. E1-Fadaly et al. [1] and J. G. Blauel et al. [28] have earlier studied J resistance of similar material. The obtained values of J are found to be, higher than those reported by M.S. E1-Fadaly et al and J. G. Blauel et al. The determination of J_{QC} by M.S. E1-Fadaly et al. and by the present author is based on unloading compliance method to obtain J-R curve, whereas fracture initiation toughness by. J. G. Blauel [28] has been detected by Direct Current Potential Difference (DCPD) method. The estimated average J-integral fracture toughness values of the steel at room temperature is 665.44 kJ/m2 (§ Table 4.4) for specimens GM-06, GM-07 and GM-09.

4.5.3 Stretch Zone Width calculation at Room Temperature

In order to understand the difference in the values of J_{IC} obtained in this investigation and that by M.S. E1-Fadaly et al. [1], the fracture surfaces of the specimen GM-04,GM-05 as shown in fig.4.12.and fig.4.13. These fracture specimens were observed in SEM. A typical representative photograph of the initial region of the ductile crack extension is shown in Fig.4.14.and fig.4.15 the fatigue pre-cracked region is found to be followed by an expanse of stretch zone (SZ), which in turn is followed by ridges of ductile crack extension. But another dark region depicting the characteristics of stretch zone is found to follow the ductile crack extension (Fig.4.14). The observed nature of the stretch zone is thus of conventional type, and it is easy to estimate the width of the stretch zone and further stable crack initiation toughness.

The width of a stretch zone (SZW) gives indication about the fracture initiation toughness of a material [21,39,47]. An attempt was made to evaluate the SZW of a GM-05 specimen. Measurements were done on a series of fractographs representing almost the entire stretch zone region across the specimen thickness

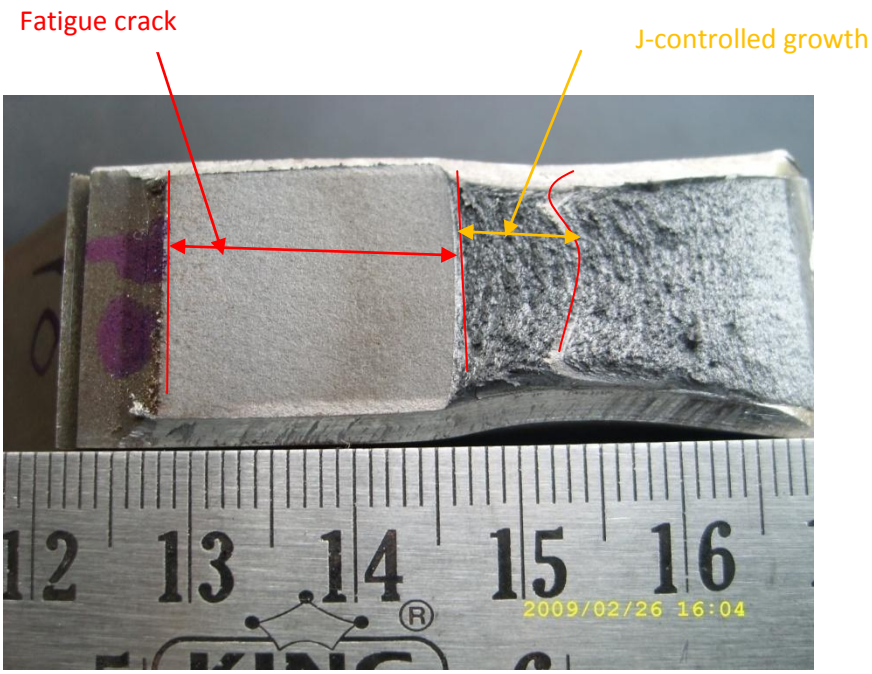

Fig.4.12 Typical fracture specimen (GM-04) of monotonic test for 20MnMoNi55 steel at room temperature Monotonic *J-R* specimen show a thumbnail shape a head of the fatigue crack.

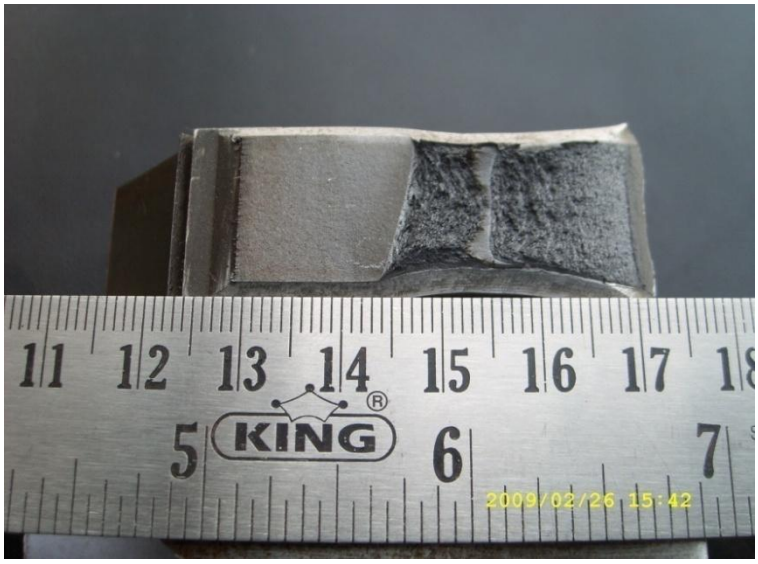

Fig.4.13. Typical fracture specimen (GM-05) of monotonic test for 20MnMoNi55 steel at room temperature. Monotonic *J-R* specimens show a thumbnail shape a head of the fatigue crack.

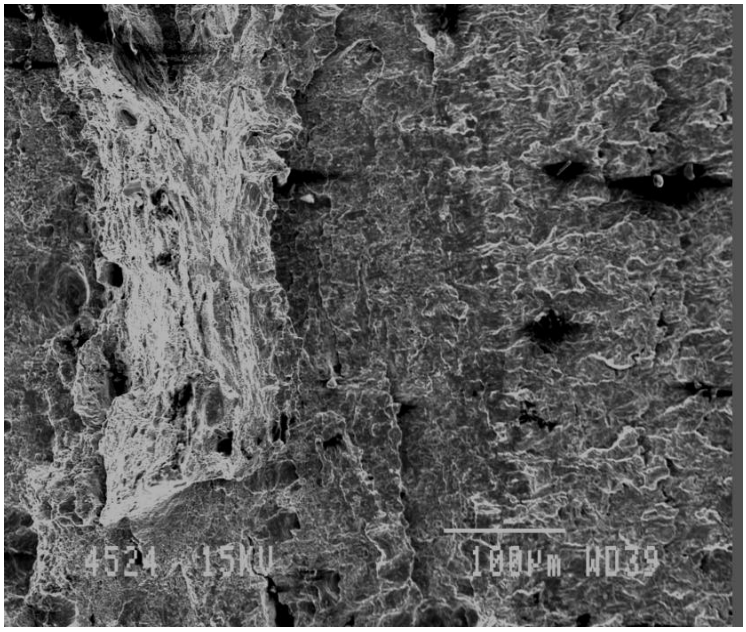

Figure.4.14. Typical SEM fractograph of SZW of J-integral tested specimen(GM-04) showing alternation stretch and void coalescence ahead of the fatigue pre-crack.

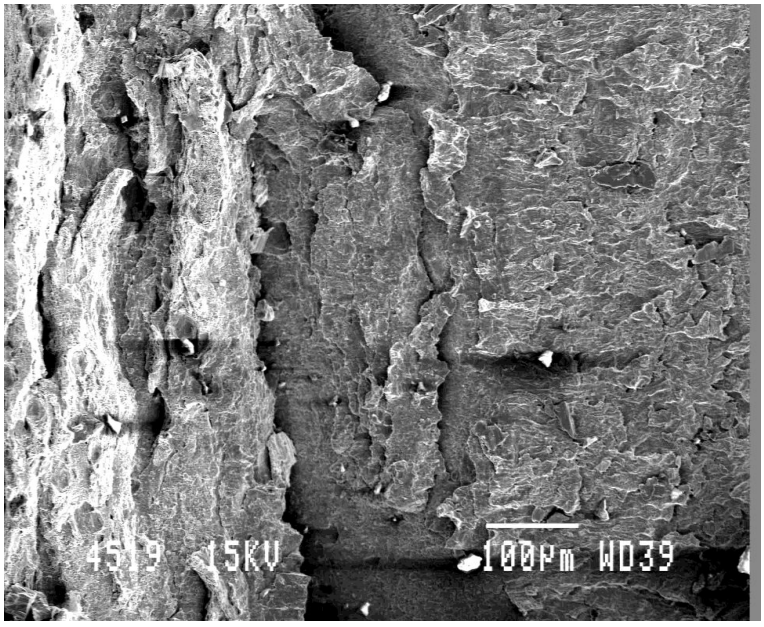

Figure.4.15. Typical SEM fractograph of SZW of J-integral tested specimen (GM-05) showing alternation stretch and void coalescence ahead of the fatigue pre-crack.

Procedure to measure the stretch zone

These fracture specimens were observed in SEM. A typical representative photograph of the initial region of the ductile crack extension is shown in Fig.4.14. Then mark the start of the stretch Zone Similarly, draw line to mark the end of SZ. Once look at several photos, eyes will get trained and get the feeling where the SZ ends. Now drawn the lines, marking start and end of SZ. Take a transparent graph sheet. Keep it under the print out of SZ with stretch zone boundaries drawn. Start measuring the distances between the start and end SZ at every 2mm or whatever interval convenient. But be uniform. Now have the micron marker in photo measure the micron marker. Now know the micron marker reading (it will be printed in SEM image) simply work the corresponding reading. If the measurement of micron marker is 10mm and number printed below the marker is 10 micron...you can work out 1mm corresponds to how many micron, Just multiply all readings by this conversion. It will give you the Stretch Zone in micron. The procedure is shown in fig.4.16.

Fracture initiation toughness can be evaluated from the J-R curve by vertical intercept at Δa = SZW on J-Δa plot as shown in Fig.4.9. The values of fracture initiation toughness (J_{SZW}) are found to be 364.02 kJ/m2 and total expanse of SZW values of 228.90 .Similarly J_{SZW} is calculated for other specimens as shown in Table.4.6.

Table.4.6. The J_{SZW} values at room temperature

Specimen code	SZW micron	J_{SZW} KJ/m^2
GM-01	256.9	424.1
GM-02	296.0	296.2
GM-03	227.8	226.8
GM-04	178.34	227.96
GM-05	228.90	364.02

Material: **20MnMoNi 55**, Specimen Code: **GM-05**

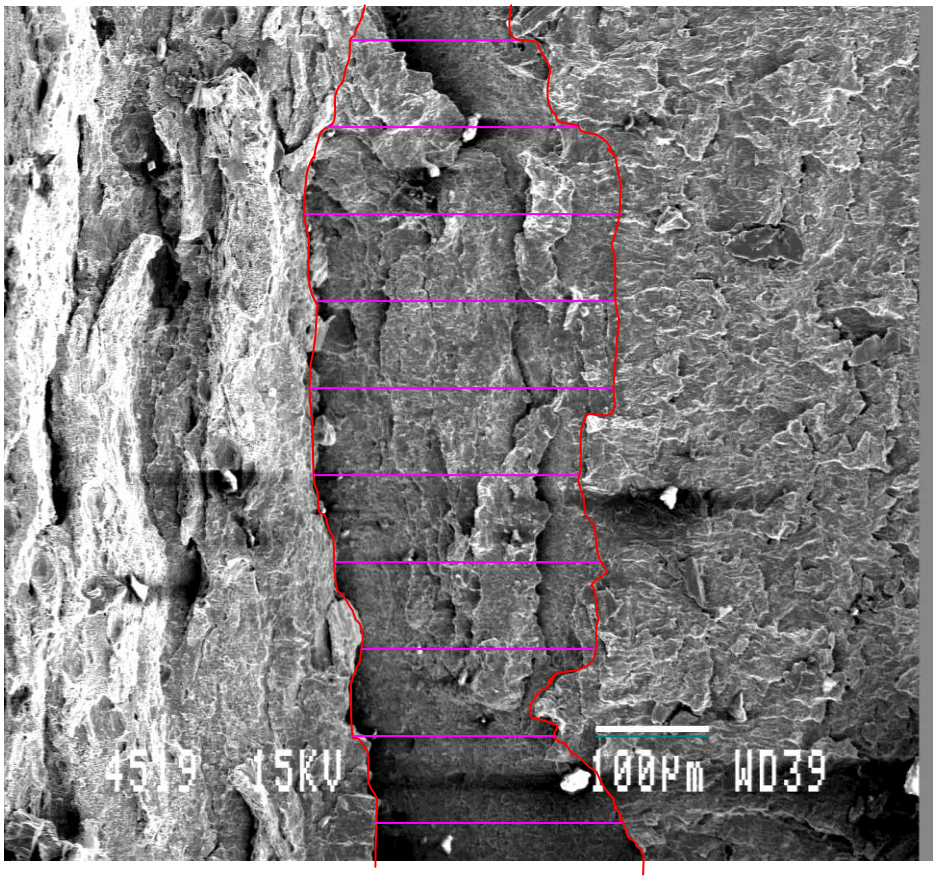

Fig.4.16 Calculation of Stretch Zone Width on SEM micrograph of monotonic fracture toughness test specimen for A 20MnMoNi55 steel (a) An horizontal lines indicates the stretch zone width (SZW) ahead of fatigue pre-crack and before actual crack growth

Sl .No	Line length(mm)	SZW(in microns)
1	25.45	160.26
2	35.56	223.93
3	44.96	283.12
4	42.21	265.80
5	42.86	265.90
6	38.1	239.92
7	37.85	238.35
8	33.36	210.07
9	28.86	181.73
10	34.93	219.96
	Average	228.90±**38.40**

Micron marker: 15.88 mm = 100 microns

J_{SZW} =364.023(KJ/m^2) , Δa =0.2289=0.23 mm

4.5.4 Fracture Toughness at Elevated Temperature

The estimated average J-integral fracture toughness values of the steel at 300^0C temperature is 665.44 kJ/m2 (§ Table 4.4) for specimens GM-06, GM-07 and GM-09. M.S. E1-Fadaly et al. [1] and J. G. Blauel et al. [28] have earlier studied J resistance of similar material. The obtained values of J_{QC} are found to be, higher than those reported by M.S. E1-Fadaly et al and J. G. Blauel et al. The determination of J_{QC} by M.S. E1-Fadaly et al. and by the present author is based on unloading compliance method to obtain J-R curve, whereas fracture initiation toughness by. J. G. Blauel [28] has been detected by Direct Current Potential Difference (DCPD) method.

In order to understand the influence of temperature on the fracture initiation toughness, the magnitudes of J_{IC} were plotted against the test temperatures. These plots are shown in Fig.4.17. It may be observed from Fig.4.17 that J_{IC} decreases linearly with increase in test temperature Other researchers have also reported similar decrease in fracture resistance of the material due to dynamic strain aging as summarized in Singh et al. [48].

4.5.5 Stretch Zone Width calculation at elevated Temperature

The fracture surfaces of the specimen GM-06, GM-07 as shown in fig.4.18.and fig.4.19. These fracture specimens were observed in SEM. The mechanism responsible for lower fracture initiation toughness at elevated temperatures was a priori searched for in terms of the nature of stretch zone. Clear demarcation of stretch zone in specimen tested at elevated temperatures was found to be difficult because of oxide layer. But some interrupted domains could be photographed. A typical representative photograph of the initial region of the ductile crack extension tested at $300^0 C$ is shown in Fig.4.20 and Fig.4.21. A comparison of this stretch zone with the one observed in specimens tested at room temperature (Fig.4.15) indicates distinct difference. The expanse of stretch zone at elevated temperature is not interrupted by ridges of ductile crack extension unlike that has been observed for specimen tested at $28^0 C$ (in Fig.4.15). It is thus considered that the absence of re-toughening of the crack tip, which increases the apparent toughness of the material at room temperature, is the cause to reflect lower toughness at elevated temperatures. However no correlation has been sought for between indirect estimates of J_{SZW} from stretch zone width and the magnitudes of J_{IC} for specimens tested at elevated temperatures because of the difficulty in reasonable estimation of SZW as discussed earlier.

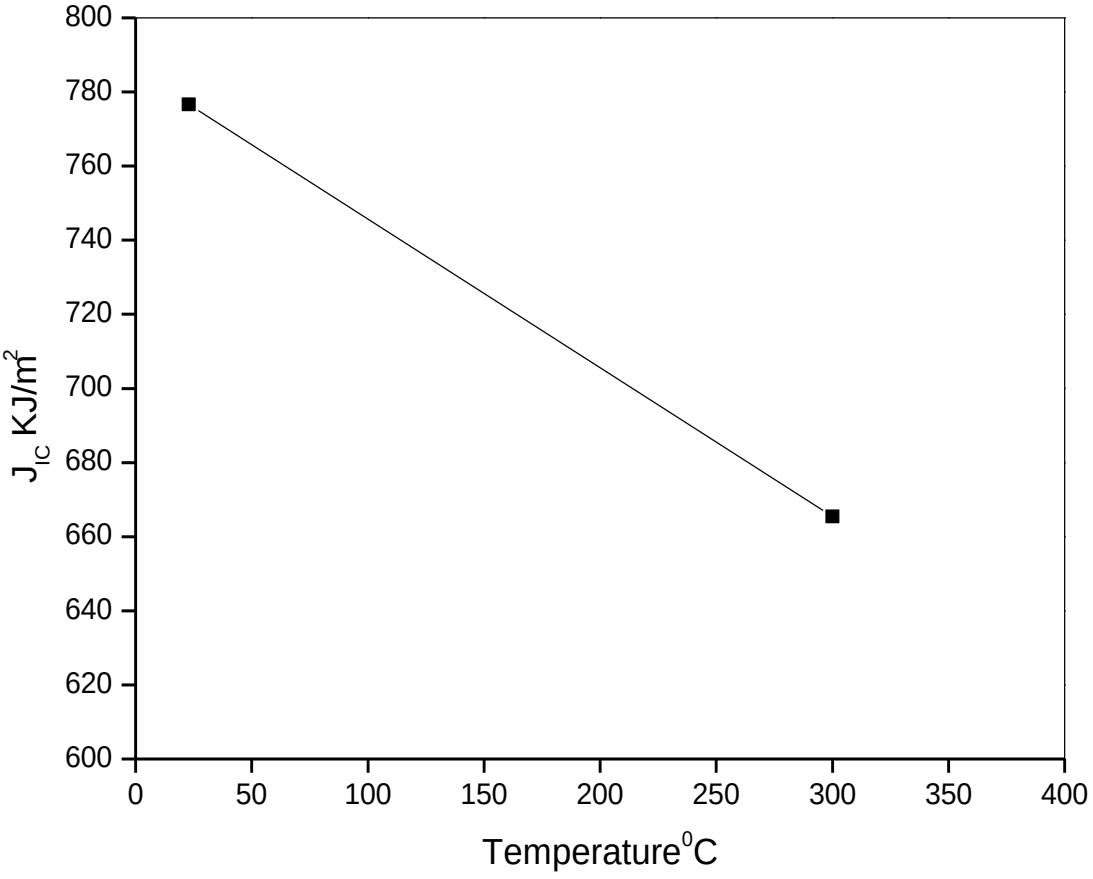

Figure.4.17. Variation of J_{IC} vs temperature at room temperature and elevated temperature

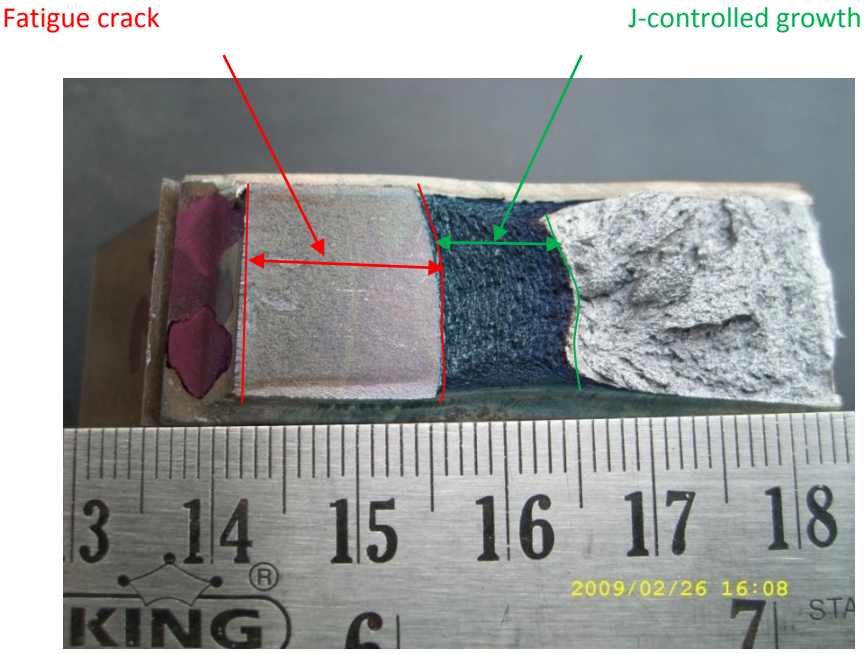

Figure.4.18. Typical fracture specimen (GM-07) of monotonic test for 20MnMoNi55 steel at elevated temperature. Monotonic *J-R* specimens show a thumbnail shape a head of the fatigue crack.

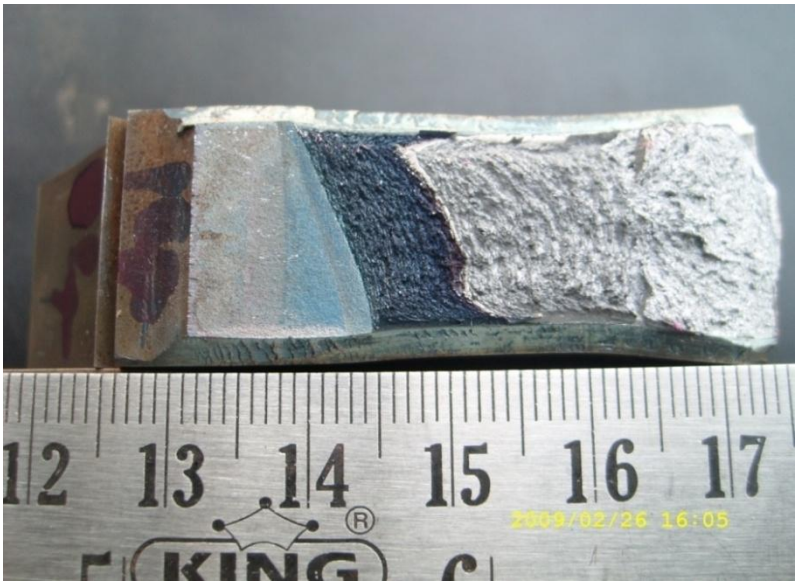

Figure.4.19 Typical fracture specimen (GM-06) of monotonic test for 20MnMoNi55 steel at elevated temperature. Monotonic *J-R* specimens show a thumbnail shape a head of the fatigue crack.

Figure.4.20. Typical SEM fractograph of SZW of J-integral tested for specimen GM-06

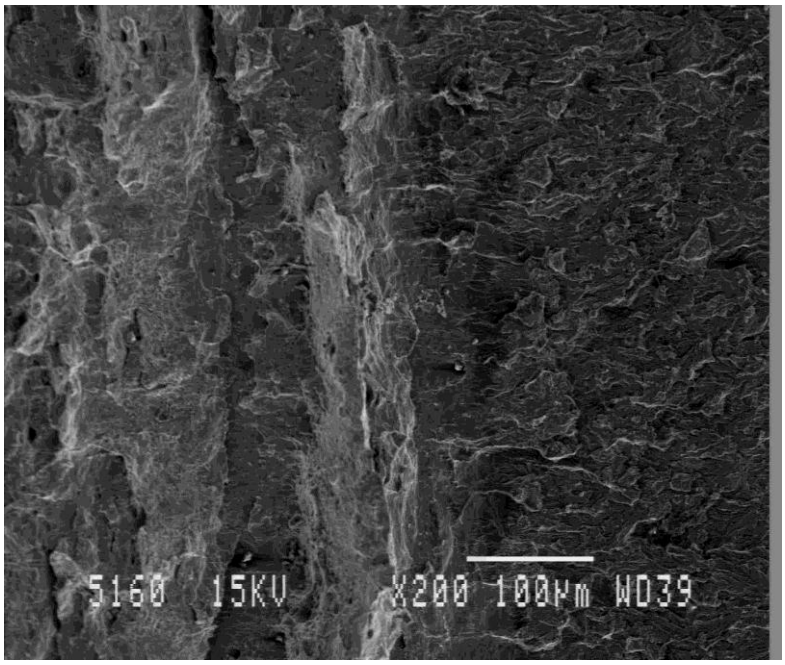

Figure.4.21 Typical SEM fractograph of SZW of J-integral tested for specimen GM-07

These fracture specimens were observed in SEM. A typical representative photograph of the initial region of the ductile crack extension is shown in Fig.4.21. Then mark the start of the stretch Zone Similarly, draw line to mark the end of SZ. Once look at several photos, eyes will get trained and get the feeling where the SZ ends. Now drawn the lines, marking start and end of SZ. Take a transparent graph sheet. Keep it under the print out of SZ with stretch zone boundaries drawn. Start measuring the distances between the start and end SZ at every 2mm or whatever interval convenient. But be uniform. Now have the micron marker in photo measure the micron marker. Now know the micron marker reading (it will be printed in SEM image) simply work the corresponding reading. if the measurement of micron marker is 10mm and number printed below the marker is 10 micron...you can work out 1mm corresponds to how many micron, Just multiply all readings by this conversion. It will give you the Stretch Zone in micron. The procedure is shown in fig.4.22.

Fracture initiation toughness can be evaluated from the J-R curve by vertical intercept at Δa = SZW on J-Δa plot as shown in Fig.4.10. The values of fracture initiation toughness (J_{SZW}) are found to be 260.65 kJ/m2 and total expanse of SZW values of 127.28 .Similarly J_{SZW} is calculated for other specimens as shown in Table.4.7.

Table.4.7. The J_{SZW} values at elevated temperature

Specimen code	SZW micron	J_{SZW} KJ/m^2
GM-06	197.74	295.40
GM-07	127.28	260.65
GM-09	98.46	264.67

Material: 20MnMoNi 55, Specimen Code: GM -06

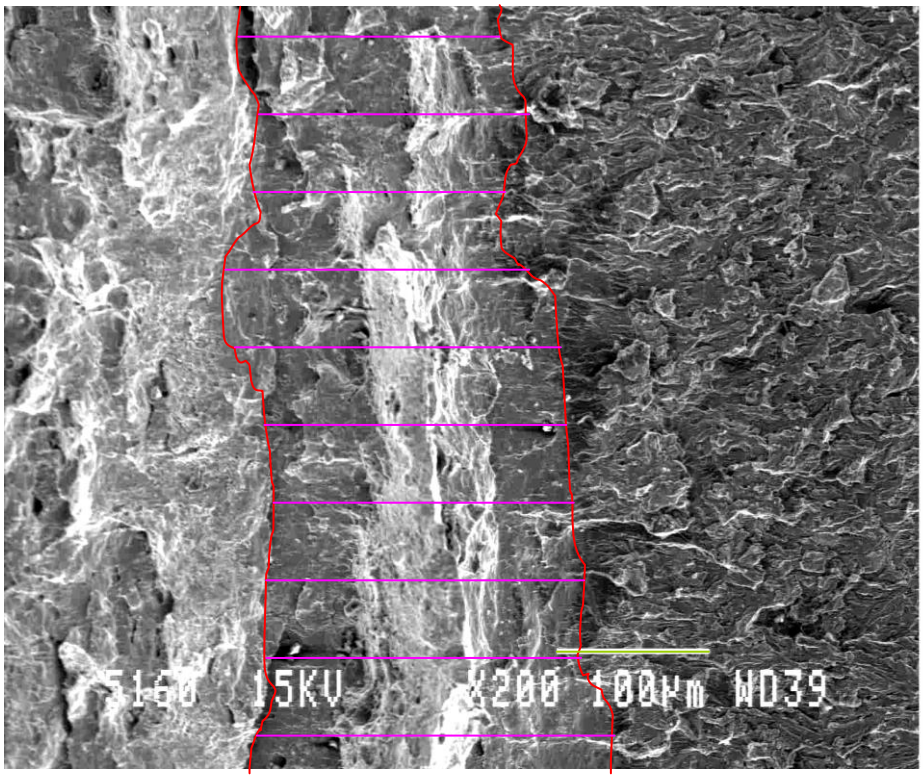

Figure.4.22. SEM micrograph of monotonic fracture toughness test specimen for a 20MnMoNi55 steel (a) An horizontal lines indicates the stretch zone width (SZW) ahead of fatigue pre-crack and before actual crack growth

Sl .No	Line length(mm)	SZW(in microns)
1	37.31	171.86
2	38.63	177.94
3	35.98	165.73
4	43.39	199.86
5	46.57	214.51
6	43.13	198.66
7	42.86	197.42
8	45.38	209.03
9	44.98	207.19
10	51.06	235.19
	Average	197.74±**21.06**

Micron marker: 21.71 mm = 100 microns

J_{SZW} =260.65$\left(KJ/m^2\right)$, Δa =0.198=0.20

CHAPTER: 5

CONCLUSION AND SUGGESTIONS FOR FUTURE WORK

5.1 Conclusion

All critical engineering applications demand assessment of the structural integrity of components in the employed service conditions for their safe operation. The Pressure vessel of pressurized heavy water reactors (PHWRs) is one such component in the nuclear power plants. This component is designed and operated on the basis of leak before break (LBB) concept. The LBB concept is based on the principles of fracture mechanics. This approach attempts to ensure that no catastrophic rupture would occur of an engineering component without prior indication of leakage. To ensure LBB concept, information and understanding of the fracture behaviour of the material used for fabrication of a component, are required. The Pressure vessels of some nuclear power plants are often made of 20MnMoNi55 steel, the material of interest in this investigation. In order to assess the structural integrity of this component understanding of the fracture resistance behaviour of 20MnMoNi55 steel up to the temperature of $300^0 C$ is required. This investigation has been directed to achieve such understanding.

The following major conclusions can be drawn from the investigations

1. The J_Q fracture toughness values of 1CT specimens prepared from the selected 20MnMoNi55 steel satisfy the validity criteria suggested in ASTM E-1820 standard. This J_Q value has to be used for LBB analysis.

2. The characteristics of the stretch zone in the investigated steel are of conventional type and it can be easily recognized. Its initial and total expanse can be used to estimate approximate values of J_i and J_{IC} respectively..

3. The magnitudes of J_{IC} of the steel estimated in the temperature of $300^0 C$ are lower than those at room temperature. This has been attributed to embrittlement tendency being operative in the above-stated temperature range

5.2 Future Work

(1) The studies carried out have helped in understanding the monotonic fracture behaviour of the steel under different test conditions, but the Pressure vessels consists of several weld joints. The fracture resistance of the weld joints would not be the same as that obtained using virgin steel. So future investigation may be directed to understand fracture behaviour of the welded joints of 20MnMoNi55 steels in the temperature range 0 to $300^0 C$. In addition it would be of great academic interest to know whether the DSA phenomenon remains prevalent in the weld joints.

(2) In the present investigation Monotonic fracture toughness studies on the steel has been carried out at ambient temperatures and elevated temperatures, future work may be directed to understand the cyclic J–R curve behaviour of the material at room temperatures and elevated temperatures. Similar work should also be done on the weld joints of 20MnMoNi55 steel.

(3) In the present investigation Monotonic fracture toughness studies on the steel has been carried out at ambient temperatures and elevated temperatures, future work may be directed to understand the monotonic J-R curve of the material at low temperatures .Similar work may be done on the weld joints of 20MnMoNi55 steel.

REFERENCES

[1]M.S. E1-Fadaly , T.A. E1-Sarrage , A.M. Eleiche , W. Dahl **, "**Fracture toughness of 20MnMoNi55 steel at different temperatures as affected by room-temperature pre-deformation" Journal of Materials Processing Technology 54 (1995) 159-165.

[2] The Determination of the fatigue crack growth in reactor pressure vessel, 4th Regional meeting , Nuclear energy in central Europe , September 7-10,1997,bled, Slovenia.

[3]M. T. Kirk, K. C. Koppenhoefer and C. F. Shih, Effect of Constraint on Specimen Dimensions Needed to Obtain Structurally Relevant Toughness Measures, in 'Constraint effects in fracture', ASTM STP 1171, Eds., E. M. Hackett, K-H. Schwalbe and R.H. Dodds, Philadelphia, PA, ASTM (1993) pp. 79-103.

[4]Griffith, A.A., "The phenomena of rupture and flow in solids", PhilosophicalTransactions, Series A, Vol. 221, 1920, pp163-198

[5]Irwin, G.R., "Fracture Dynamics", Fracturing of Metals, American society of metals, Cleveland, 1948,p 147-166.

[6]Rice J.R.," a path independent integral and approximate analysis of strain concentration by notches and cracks", Journal of Applied Mechanics, Vol.35, 1968, pp379-386

[7] Wells, A. A, British Welding Research Ass. Rep M13, 1963.

[8]R.W.Hertzberge, Deformation and Fracture Mechanics of Engineering Materials, 3rd Edition, John Wiley and Sons, Singapore, 1989.

[9] G.E. Dieter, "Mechanical Metallurgy "McGraw-Hill Book Company.. 1998.

[10**]** Kraft, J.M., Sullivan, A.M. and Boyle, R.W., Proc. Crack Propagation Symp., Cranfield, 1, p8, 1961.

[11] Barr, W., "The fracture of Metals", Inst. of Metallurgist, p. 117, 1950.

[12] Irvine, K.J. "Strong Tough structural steel", Iron and Steel Inst. Publ. 104, 1967.

[13] Keehan, E., and Andren, H. O."Microstructural and mechanical effects of nickel and manganese on high strength steel weld metals", Chalmers University of Technology, Gothenburg, Sweden. Technical paper 2002.

[14]Young, Im. “Effect of Carbide Precipitation on the Strength and Charpy Impact Properties of Low Carbon Mn- Ni- Mo Bainitic Steels”, Journal of Nuclear Materials, 297, pp138-148. 2001.

[15] Bhole, S.D., Nemade, J.B., Collin, L., and Liu, Cheng., [2006], “Effect of nickel and molybdenum additions on weld metal toughness in a submerged arc welded HSLA line-pipe steel” Journal of Materials Processing Technology, 173, pp 92–100

[16]Pickering F.B**.,** [1977], “The structure and properties of banite in steels, in transformation and hardenability in Steels”, Climax Molybdenum Company of Michigan, Ann Arbor, MI, p 109-132.

[17] Das, S.K., Sivaprasad, S., Das, S., Chatterjee, S. and Tarafder S**.** [2006]**,** “The effect of variation of microstructure on fracture mechanics parameters of HSLA-100 steel”, Materials Science and Engineering, A 431, pp 68–79.

[18]H. Roy, S. Sivaprasad, S. Tarafder, K.K. Ray, Monotonic vis-à-vis cyclic fracture behavior of AISI 304LN stainless steel, Engineering Fracture Mechanics (2009).

[19] M. Nabil Bassim**,** Use of the stretch zone for the characterization of ductile fracture Journal of Materials Processing Technology 54 (1995) 109-113.

[20] P. Nguyen-Duy and S. Bayard, J. Eng. Mats. Tech. 103 (1976) 301.

[21]Tarafdar. S., Ranganath V. R., Sivaprasad. S. and Johri. P., “Ductile fracture behaviour of primary heat transport piping material of nuclear reactors”, Sadhana, Volume 28, part 1 & 2, February/April 2003, Pages 167–186.

[22]Chattopadhyay J., Dutta B.K. and Kushwaha H.S**.** , “Evaluation of J-R Curve of Through wall Cracked Elbow Under In-plane Bending Moment “ RSD, Hall-7, Bhabha Atomic Research Centre, Mumbai - 400085, India

[23] Chattopadhyay J., Kushwaha H.S. , Roos E. **, “**Some recent developments on integrity assessment of pipes and elbows” Part II: Experimental investigations a Reactor Safety Division, Hall-7, Bhabha Atomic Research Centre, Mumbai 400085, India ,b Material Testing Institute, MPA, Pfaffenwaldring 32, University of Stuttgart, D-70569 Stuttgart, Germany

[24] Chattopadhyay J., Pavankumar T.V., Dutta B.K., Kushwaha H.S., "Fracture experiments on through wall cracked elbows under in-plane bending moment: Test results and theoretical/numerical analyses" 'Reactor Safety Division, Hall-7, Bhabha Atomic Research Center, Mumbai 400085, India.

[25] ASTM E813, Standard Test for J_{IC}, a measure of Fracture Toughness, American Society for Testing and Materials, Annual Book of ASTM, Standards, 1987.

[26]ASTM E399, Standard Test Method for Plan Strain Fracture Toughness of Metallic Materials, Annual Book of ASTM Standards, Section 3, 1983.

[27] B. Voss and R.A. Maguille, The Use of the Partial Unloading Compliance Method for the Determination of J-R Curves and J_{IC}, Elastic-Plastic Fracture Test, ASTM STP 856, 1985 p. 117.

[28] J. G. Blauel, L. Hodulak, T. Hollstein & B. Voss **,** **"**Material Characterization by J-R Curves of a 20MnMoNi55 Forging " Int. J. Pres. Ves. & Piping 17 (1984) 139-162

[29 E813-89, standard test methods for J_{IC}, a measure of fracture toughness. In: Annual book of ASTM standard, Vol. 03.01. Philadelphia, PA: ASTM, 1992:732-745.

[30]P.K. Singh, J. Chattopadhyay, H.S. Kushwaha **,** **"**Tensile and fracture properties evaluation of PHT system piping material of PHWR "International Journal of Pressure Vessels and Piping 75 (1998) 271-280.

[31] E l152-87**,** standard test methods for determination of J-R curve. In: Annual book of ASTM standard, Vol. 03.01. Philadelphia, PA: ASTM, 1992:847-857.

[32]Andrew WR, Park GA, Paris PC, Schimdt DW. Single specimen test for J_{IC} determination; mechanics of crack growth. ASTM-STP 590. Philadelphia, PA: ASTM, 1976:27-42.

[33] Mukherjee B. The J-resistance curve LBB test program on material for the Darlington nuclear generating station. Int. J Pres. Ves. and Piping, 1988;31:363-385.

[34] Kim YJ et al. Fracture toughness data for carbon steel piping material. Int. J Pres. Ves. and Piping, 1996; 68:209-217.

[35] C.R. Chen et al**. /** Engineering Fracture Mechanics 72 (2005) 2072–2094 2093.

[36] L.V. Vareda, D. Spinelli Fatigue, monotonic and fracture toughness properties of a Cr–Mn–N steel, International Journal of Fatigue 23 (2001) 857–863.

[37] K. Mogami, T. Hayashi, K. Ando & N. Ogura Elastic-Plastic Fatigue-Crack Growth and Tearing Instability Behavior under Cyclic Loads , Int. J. Pres. Ves. & Piping 44 (1990) 85-97.

[38] Y. Nakajima , Fracture toughness behaviour of service-exposed type 321 stainless steel at room and elevated temperature under normal and low straining rates Engineering Fracture Mechanics, Volume 33, Issue 2, 1989, Pages 295-307.

[39]S.Sivaprasad, S.Tarafder, V.R.Ranganath, and K.K Ray, Modeling ductile fracture behaviour from deformation parameters in HSLA steels. National Metallurgical Laboratory, Jamshedpur, India. (2004).

[40] E. Roos , M. Seidenfuss , D. Kraimer , S. Krolop , U. Eisele and U. Hindenlang , Application and evaluation of different numerical methods for determining crack resistance curves , Nuclear Engineering and Design 130 (1991) 297-308.

[41] K.Bruninghaus, J.Falk, M.Twickler and W.Dahil, Determination of crack resistance curves under static and dynamic loading by analysis of load displacement relationship, Engineering Fracture mechanics Vol. 34. No. 4, pp. 989-1000, 1989.

[42] H. Roy, S. Sivaprasad, S. Tarafder, K.K. Ray, Monotonic vis-à-vis cyclic fracture behaviour of AISI 304LN stainless steel, Engineering Fracture Mechanics (2009),

[43] E 8M-94a, Test Methods for Tension Testing of Metallic Materials (Metric), Annual Book of ASTM Standards, Vol.03.01, p.81-100, ASTM, Philadelphia, PA, 1994

[44]E 399-90, Test method for Plane-Strain Fracture Toughness of Metallic Materials, Annual Book of ASTM Standards, 1994, Vol.03.01, pp.407-437, ASTM, Philadelphia, PA

[45]E 647-93, Standard Test Method for Measurement of Fatigue Crack Growth Rates, Annual Book of ASTM Standards, 1994, Vol.03.01, pp.569-596, ASTM, Philadelphia, PA.

[46]E1820-08a Standard test method for Measurement of Fracture Toughness, Annual Book of ASTM Standards, Vol.03.01, p.1-34, ASTM, Philadelphia, PA, 2008

[47]M.Srinivas, S.V.Kamat and P.Rama Rao, J. of testing and Evaluation. 22, No4, pp 302-308, July 1994.

[48] P.K.Singh , J.Chattopadhaya, H.S.Kushwaha, S.Trafder and V.R. Ranganath Int.J of Press.Ves & Piping, vol 75, p271, 1998